NWC TP 6363

An Introduction to Velocity Coupling in Solid Propellant Rockets

by
F. E. C. Culick
Research Department

FEBRUARY 1983

NAVAL WEAPONS CENTER
CHINA LAKE, CALIFORNIA 93555

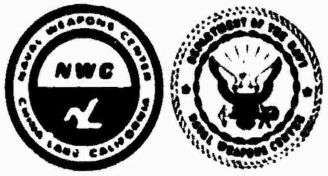

Naval Weapons Center
AN ACTIVITY OF THE NAVAL MATERIAL COMMAND

FOREWORD

The intent of this report is to provide a complete and coherent framework in one publication of the currently known principles governing the phenomenon commonly called "velocity-coupled combustion instability." As the report evolved, the basic ideas were fitted into the analytical framework of solid propellant combustion instability which has developed considerably in the recent past. The results, among other things, provide a simplified analysis for measuring the velocity-coupled propellant response function using a modified T-burner.

This work was sponsored by the Naval Air Systems Command under NAVAIR Propulsion Block Task WF31.300.00 and was performed during the period October 1980 to September 1982.

This report is transmitted for information only and does not represent the official views or final judgment of the Center.

This report was reviewed for technical accuracy by H. B. Mathes.

Approved by
E. B. ROYCE, *Head*
Research Department
28 February 1983

Under authority of
J. J. LAHR
Capt. U.S. Navy
Commander

Released for publication by
B. W. HAYS
Technical Director

NWC Technical Publication 6363

Published by . . . . . Technical Information Department
Collation . . . . . Cover, 32 leaves
First printing . . . . . 310 unnumbered copies

UNCLASSIFIED

SECURITY CLASSIFICATION OF THIS PAGE (When Data Entered)

REPORT DOCUMENTATION PAGE		READ INSTRUCTIONS BEFORE COMPLETING FORM
1. REPORT NUMBER NWC TP 6363	2. GOVT ACCESSION NO.	3. RECIPIENT'S CATALOG NUMBER
4. TITLE (and Subtitle) AN INTRODUCTION TO VELOCITY COUPLING IN SOLID PROPELLANT ROCKETS		5. TYPE OF REPORT & PERIOD COVERED ANALYSIS 1980-1982 6. PERFORMING ORG. REPORT NUMBER
7. AUTHOR(s) F. E. C. Culick		8. CONTRACT OR GRANT NUMBER(s)
9. PERFORMING ORGANIZATION NAME AND ADDRESS Naval Weapons Center China Lake, CA 93555		10. PROGRAM ELEMENT, PROJECT, TASK AREA & WORK UNIT NUMBERS NAVAIR PROPULSION BLOCK TASK WF31.300.00
11. CONTROLLING OFFICE NAME AND ADDRESS Naval Weapons Center China Lake, CA 93555		12. REPORT DATE February 1983 13. NUMBER OF PAGES 60
14. MONITORING AGENCY NAME & ADDRESS(if different from Controlling Office)		15. SECURITY CLASS. (of this report) UNCLASSIFIED 15a. DECLASSIFICATION/DOWNGRADING SCHEDULE

16. DISTRIBUTION STATEMENT (of this Report)

APPROVED FOR PUBLIC RELEASE; DISTRIBUTION UNLIMITED.

17. DISTRIBUTION STATEMENT (of the abstract entered in Block 20, if different from Report)

18. SUPPLEMENTARY NOTES

19. KEY WORDS (Continue on reverse side if necessary and identify by block number)

COMBUSTION INSTABILITY
SOLID PROPELLANT COMBUSTION
PROPELLANT RESPONSE FUNCTION
VELOCITY COUPLING
VELOCITY COUPLED RESPONSE
VELOCITY COUPLED T-BURNER

20. ABSTRACT (Continue on reverse side if necessary and identify by block number)

See back of form.

DD FORM 1 JAN 73 1473 EDITION OF 1 NOV 65 IS OBSOLETE
S/N 0102-LF-014-6601

UNCLASSIFIED

SECURITY CLASSIFICATION OF THIS PAGE (When Data Entered)

(U) *An Introduction to Velocity Coupling in Solid Propellant Rockets*, by F. E. C. Culick, China Lake, California, Naval Weapons Center, February 1983, 60 pp. (NWC TP 6363, publication UNCLASSIFIED.)

(U) This report is a review of the principles of velocity coupling as a mechanism for sustaining pressure oscillations in solid propellant rockets. It is intended as an introduction to the fundamentals of the subject, including current analysis of linear and nonlinear acoustics. Some results are given for the influence of rectification when there is no threshold velocity. As an example, a simplified analysis is given for a T-burner having lateral grains for measuring velocity coupling.

CONTENTS

Figures:

1. INTRODUCTION AND GENERAL NOTIONS

The purpose of this report is to provide a brief review of the principles governing the phenomenon commonly called "velocity-coupled combustion instability." Most of the basic ideas covered here originated many years ago.[1-3] They have been clarified by subsequent work and the analytical framework into which they fit has developed considerably in the recent past.

So far as practical applications are concerned, the general problem of velocity coupling remains largely unsolved. The most difficult obstacles are associated with the experimental work required to produce the values of certain characteristic quantities arising in the analysis. No consideration will be given to those matters or to the details of the combustion processes and origins of the physical behavior.

Velocity-coupled combustion instability is most simply described as the behavior under unsteady conditions corresponding to erosive burning in steady flow. Observations of burning solids have established that in steady state, the regression rate is dependent on both the pressure of the environment and on the rate of flow parallel to the surface. For the purposes here it is adequate to assume that the burning increases if either the pressure or the parallel flow, or both, are increased, as sketched in Figure 1. The symbol $V_{\parallel}$ denotes the velocity parallel to the surface; often the mass flow is used as the independent variable, but the velocity will serve well enough here to develop the principles.

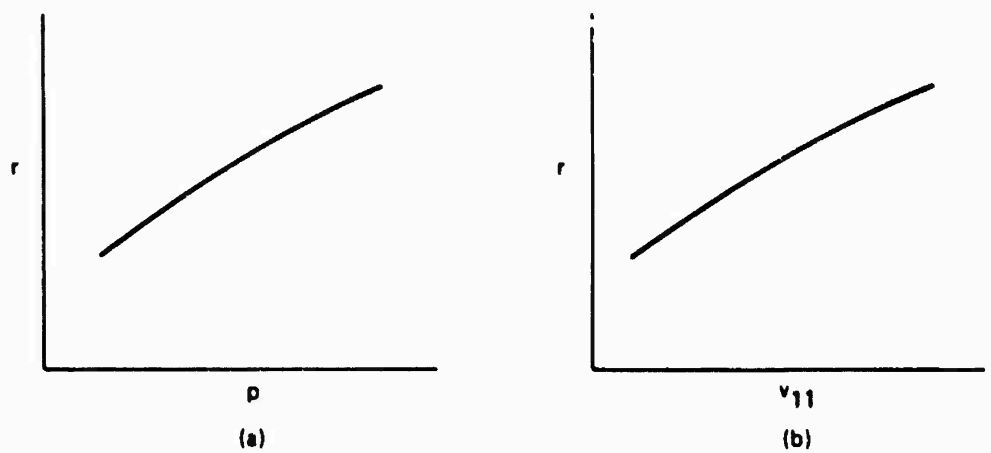

FIGURE 1. Influences of Pressure and Parallel Velocity on the Linear Burning Rate.

Now imagine that, from some initial steady operating point, the pressure is slowly changed by an amount δp. If $r \sim p^n$, then to first order in small quantities, the corresponding change in burn rate is given by

$$\frac{\delta r}{\bar{r}} = n \frac{\delta p}{\bar{p}} \tag{1}$$

where $\bar{r}$, $\bar{p}$, are the initial steady values. Obviously δp can be positive or negative, and if the pressure slowly oscillates (i.e., with very low frequency or long period) about its average value, then so does the burning rate. Similar behavior occurs if the parallel velocity is changed. Figure 2 shows schematically these quasi-steady responses of the regression rate to oscillations of pressure and velocity. Figure 3 shows the pressure, velocity, and burning rate as functions of time for the two cases. Note that for slow quasi-steady oscillations, the burning rate is always in phase with whatever independent variable is changed, providing the burning rate increases monotonically with the variable under steady conditions. We restrict ourselves here to the simplest situation in which only one variable changes and when the velocity fluctuation is smaller than the average velocity.

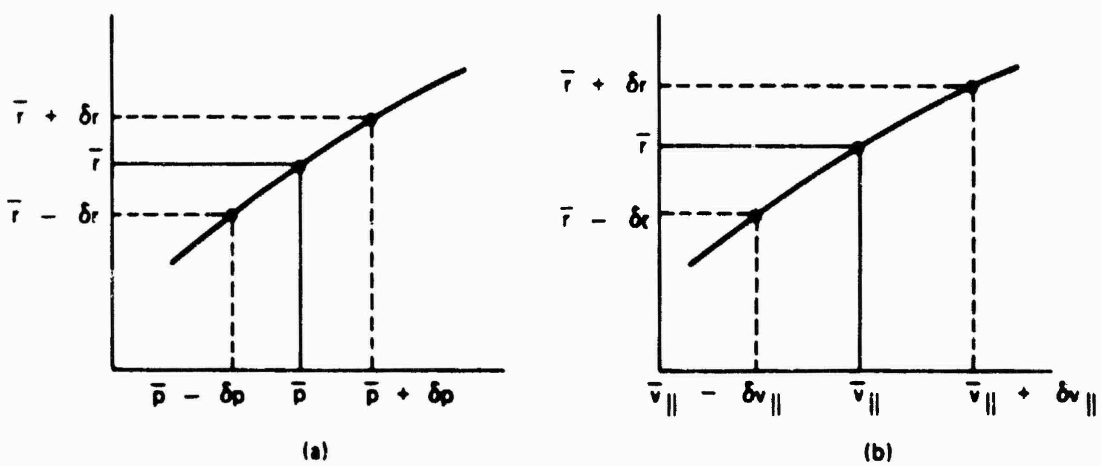

FIGURE 2. Quasi-Steady Changes of the Linear Burning Rate.

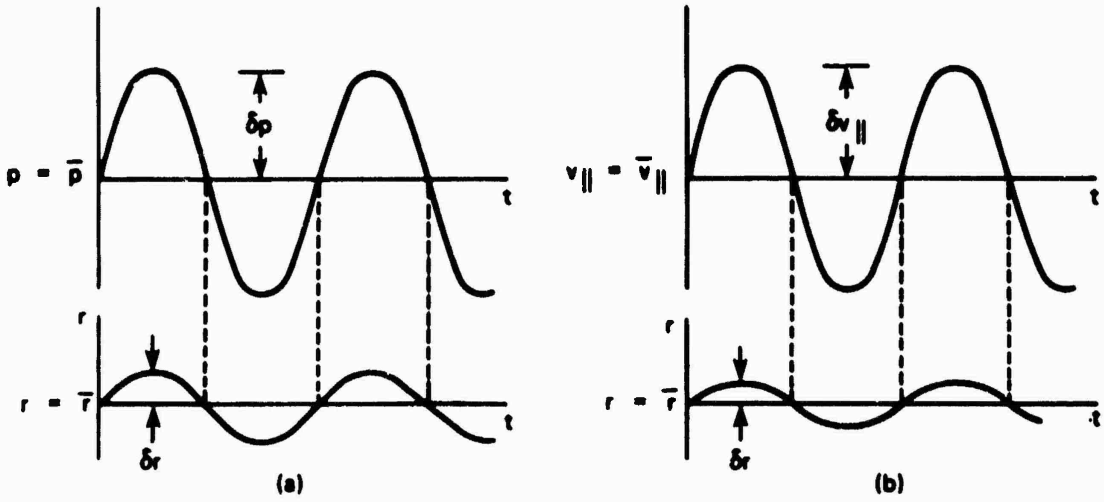

FIGURE 3. Quasi-Steady Oscillations of the Linear Burning Rate.

Consider now the situation in a combustion chamber. Suppose that for some reason the chamber pressure $\bar{p}$ is changed and that the propellant surfaces are so oriented (e.g. as in an end burner) that fluctuations of the parallel velocity are negligible. When the pressure increases, so does the burning rate, which causes the total mass of combustion products in the chamber to be increased. If no other process occurred, the pressure would be further increased, an unstable situation. Of course in practice, the increased chamber pressure causes the exhaust flow to increase, compensating for the increased burning rate; it is then a familiar result that if $n < 1$, the flow in the chamber is stable to fluctuations of pressure when the exhaust nozzle is choked. This is the quasi-steady limit of "L*" or "bulk mode" instability.

Similar considerations apply to the case when the chamber pressure is held constant, but the parallel velocity changes. The condition for stability is then not so simply stated and will not be worked out here. However, it is clear that for the cases sketched above, an increase of parallel velocity will cause an increase in the rate of mass addition to the chamber. In the absence of other processes, this will cause an increase of chamber pressure. The assumed constraint of constant chamber pressure will therefore be satisfied only if other processes, including the exhaust flow, are accounted for.

In any practical situation, changes of the velocity parallel to the surface will not occur alone: they will be accompanied by changes of pressure as well. Moreover, the geometry of combustion chambers is such that a quasi-steady increase of pressure, uniform in the chamber, will

produce a quasi-steady increase of parallel velocity everywhere. The latter will of course not generally be uniform over the burning surface. However, for small fluctuations, the total change of burning rate will be the sum of the changes due to the fluctuations of pressure and velocity. This behavior is sketched for one position on the burning surface in Figure 4.

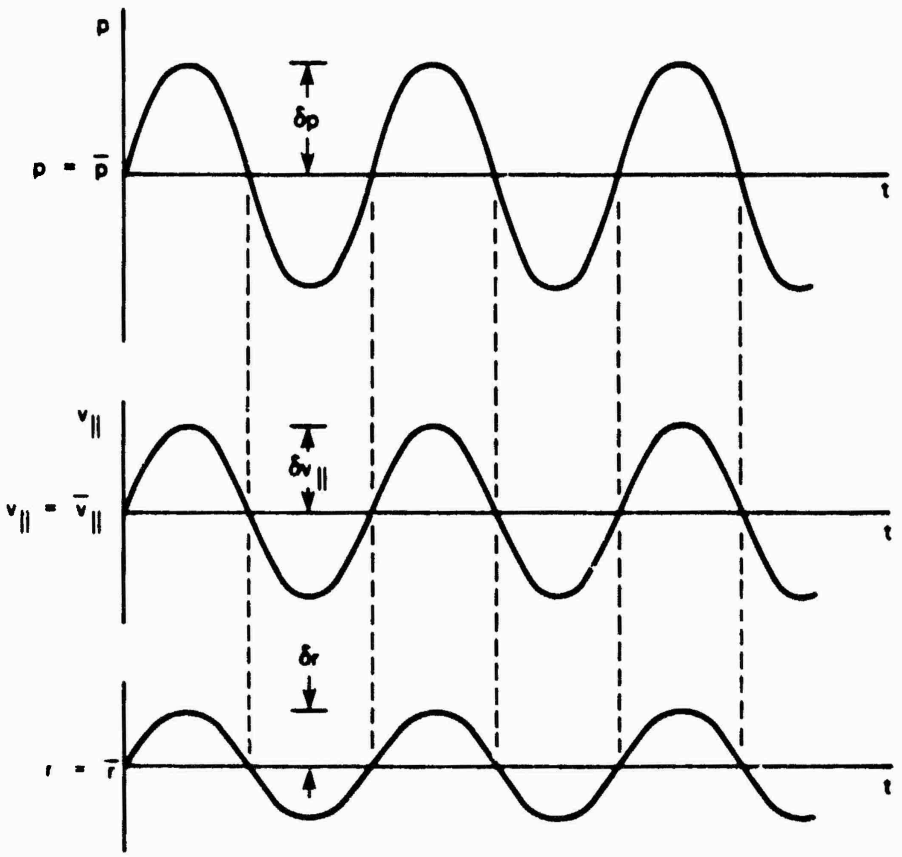

FIGURE 4. Quasi-Steady Oscillations in Response to Both Pressure and Velocity.

Qualitative examination of quasi-steady behavior is evidently straightforward, although the details of a particular case may become tedious. Under truly unsteady conditions, at higher frequencies, the analysis becomes considerably more involved. However, one principle* is always true: an increase of local burning rate with an increase of local pressure is a destabilizing influence. Thus it is that part of the burning rate in phase with the fluctuations of pressure which may produce unstable motions in the chamber. This is true whatever may be the cause for the burning rate to change.

All arguments concerning the influence of velocity coupling on combustion instability have been based on the principle stated in the preceding paragraph. What sometimes obscures the issue is the necessity to introduce some representation of the way in which the unsteady burning rate is connected to velocity fluctuations. This problem will be treated later in greater detail but it may be helpful here to outline some of the main points. We shall consider the simplest and most important case of longitudinal (axial) acoustic modes in a straight chamber. Even with combustion, particulate matter in the gases, average flow, exhaust nozzle, and other features of a real motor, the unsteady motions usually found may be regarded in good approximation as acoustical motions in a chamber having the same shape, enclosed by a rigid boundary excluding the nozzle volume and without all perturbations associated with combustion. Thus we may consider the lateral burning surface to be subject to classical acoustic modes appropriate to a closed/closed tube; the pressure field for a standing wave is proportional to $\bar{p}\cos(k_n z)\cos(\omega_n t)$ where $k_n = n\pi/L$ and $\omega_n = \bar{a}k_n$ $(n = 0,1,2,\ldots)$. To be definite, we restrict our attention to the fundamental or first axial mode having amplitude ε, the maximum value of $p'/\bar{p}$:

$$p'(z,t) = \varepsilon\bar{p}\cos\left(\pi\frac{z}{L}\right)\cos\left(\frac{\pi\bar{a}}{L}t\right) \tag{2}$$

The momentum equation for acoustical motions is

$$\bar{\rho}\frac{\partial u'}{\partial t} = -\frac{\partial p'}{\partial z} \tag{3}$$

*It will be shown in Section 2.2 that this principle is closely related to "Rayleigh's Criterion", a statement concerning the influence of heat addition on the stability of acoustic waves.

and with equation (1)

$$\bar{\rho} \frac{\partial u'}{\partial t} = \varepsilon \bar{p} \frac{\pi}{L} \sin \left(\frac{\pi}{L} z\right) \cos \left(\frac{\pi \bar{a}}{L} t\right)$$

This is easily integrated to give

$$u'(z,t) = \varepsilon \frac{\bar{a}}{\gamma} \sin \left(\frac{\pi}{L} z\right) \sin \left(\frac{\pi \bar{a}}{L} t\right) \tag{4}$$

which can be written to show explicitly the phase difference between the pressure and velocity:

$$u'(z,t) = \varepsilon \frac{\bar{a}}{\gamma} \sin \left(\frac{\pi}{L} z\right) \cos \left(\frac{\pi \bar{a}}{L} t - \frac{\pi}{2}\right) \tag{5}$$

Comparison of equations (2) and (5) shows that for $z < L/2$, the velocity lags the pressure in time by $\pi/2$. To appreciate these formulas it is helpful first to sketch the pressure and velocity mode shapes at quarter cycle intervals (Figure 5). It is also useful to have the pressure and velocity fluctuations as functions of time in the two regions $z < L/2$ and $z > L/2$ which may be regarded as the fore and aft sections of a rocket motor. These are sketched in Figure 6.

It is apparent that the velocity lags the pressure by $\pi/2$ in the head-end ($0 < z < L/2$) of the chamber and leads the pressure by $\pi/2$ in the aft-end. The reason why the phase difference depends on position in the chamber may be seen from Figure 5. For the fundamental mode, the velocity is always zero at the ends only, while the pressure field has a node at the center. Thus, although the velocity at any given instant is in the same direction throughout the chamber--i.e., has the same sign--the pressure changes sign. That sign change is reflected in the phase difference sketched above.

Now let us consider the response of a burning surface to such an acoustic field. We shall base the discussion on several assumptions:

(1) The burning rate is proportional to the pressure fluctuation for pressure coupling;

(2) The burning rate is proportional to the velocity fluctuation for velocity coupling;

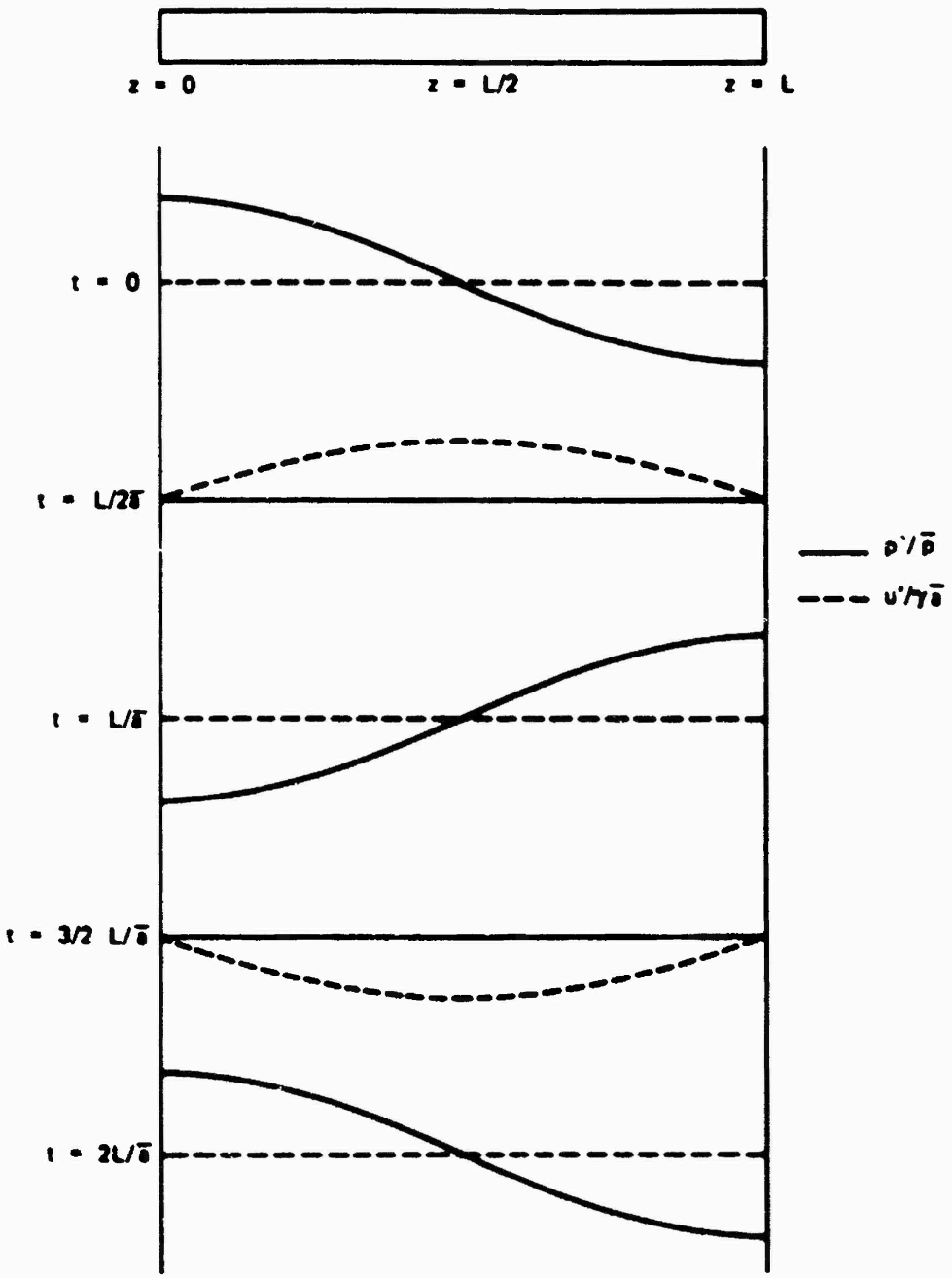

FIGURE 5. Pressure and Velocity Fluctuations in the Fundamental Longitudinal Mode.

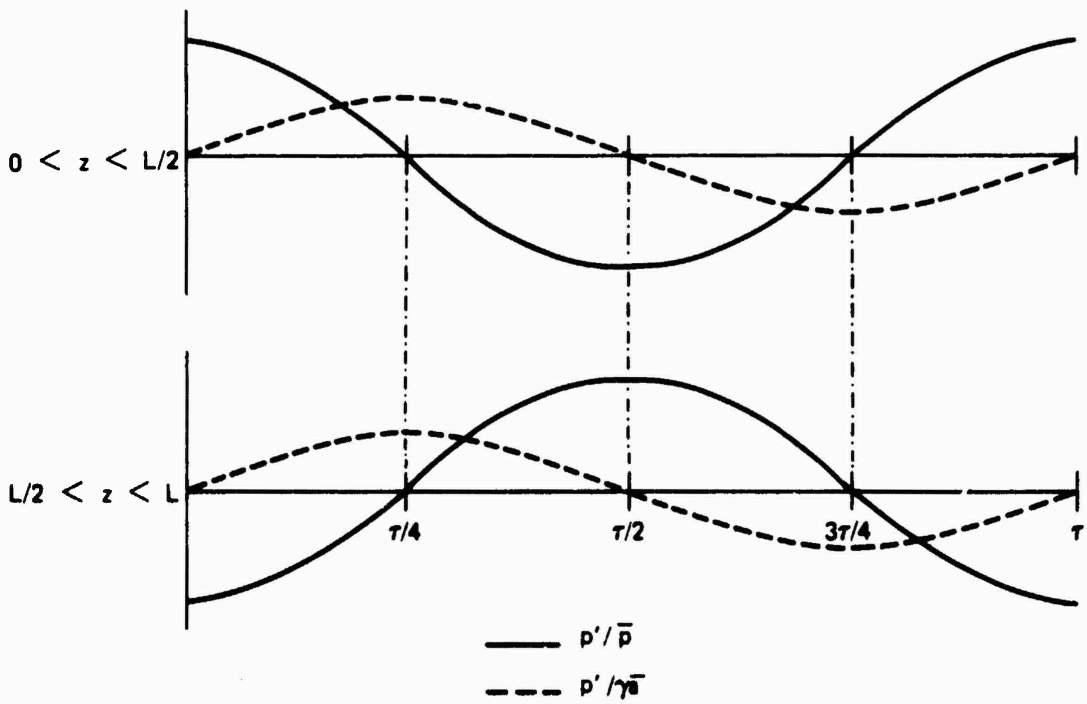

FIGURE 6. Pressure and Velocity Oscillations in the Fore and Aft Regions of a Tube.

(3) Pressure and velocity coupling are independent and linearly additive;

(4) The proportionality constants for pressure and velocity coupling are, in general, functions of frequency and contain the fact that the change of burning rate is not in phase with the pressure and velocity fluctuations. For the present, rectification is ignored, but will be discussed later.

There are several equivalent ways to write the oscillations of burning rate (items (1) and (2)). The most efficient representation involves complex notation. For the pressure field, write

$$\frac{p'}{\bar{p}} = \frac{\hat{p}}{\bar{p}} e^{i\omega t} \tag{6}$$

$$\frac{\hat{p}}{\bar{p}} = \varepsilon \cos\left(\frac{\pi z}{L}\right) \tag{7}$$

It is necessary to choose a definition of zero phase and maintain that definition consistently throughout. Unless otherwise specified, we shall follow the generally accepted convention that all phases are measured with respect to the pressure oscillation so $\hat{p}/\bar{p}$ is always real. The actual (observable) values are found by taking real parts, for then equation (2) follows from equations (6) and (7). The velocity is:

$$\frac{u'}{\bar{a}} = \frac{\hat{u}}{\bar{a}} e^{i\omega t} \tag{8}$$

$$\frac{\hat{u}}{\bar{a}} = -i \frac{\varepsilon}{\gamma} \sin\left(\pi \frac{z}{L}\right) = i\left(\frac{\hat{u}}{\bar{a}}\right)^{(i)} = e^{i\frac{\pi}{2}} \left(\frac{\hat{u}}{\bar{a}}\right)^{(i)} \tag{9a}$$

where

$$\left(\frac{\hat{u}}{\bar{a}}\right)^{(i)} = -\frac{\varepsilon}{\gamma} \sin\left(\pi \frac{z}{L}\right) \tag{9b}$$

Note that because the acoustic velocity lags the pressure by $\pi/2$, $\hat{u}/\bar{a}$ is imaginary. Define the response functions for pressure and velocity coupling:

$$R_b = R_b^{(r)} + iR_b^{(i)} = |R_b| e^{i\psi_b} = |R_b| \cos\psi_b + i|R_b| \sin\psi_b \tag{10}$$

$$R_v = R_v^{(r)} + iR_v^{(i)} = |R_v| e^{i\psi_v} = |R_v| \cos\psi_v + i|R_v| \sin\psi_v \tag{11}$$

Then the changes of burning rate due to pressure and velocity coupling are represented as

$$\left(\frac{r'}{\bar{r}}\right)_b = R_b \frac{p'}{\bar{p}} = |R_b| \frac{\hat{p}}{\bar{p}} e^{i(\omega t+\psi_b)} \tag{12}$$

$$\left(\frac{r'}{\bar{r}}\right)_v = R_v \frac{u'}{\bar{a}} = |R_v|\left(\frac{\hat{u}}{\bar{a}}\right)^{(i)} e^{i(\omega t+\psi_v + \frac{\pi}{2})} \tag{13}$$

The real parts of these are:

$$\left(\frac{r'}{\bar{r}}\right)_p^{(r)} = |R_b|\frac{\hat{p}}{\bar{p}} \cos(\omega t + \psi_b)$$

$$= |R_b| \cos\psi_b \frac{\hat{p}}{\bar{p}} \cos\omega t - |R_b| \sin\psi_b \frac{\hat{p}}{\bar{p}} \sin\omega t \tag{14}$$

$$\left(\frac{r'}{\bar{r}}\right)_{(v)}^{(r)} = |R_v|\left(\frac{\hat{u}}{\bar{a}}\right)^{(i)} \cos(\omega t + \frac{\pi}{2} + \psi_v)$$

$$= |R_v|\left(\frac{\hat{u}}{\bar{a}}\right)^{(i)} [\cos(\omega t + \frac{\pi}{2}) \cos\psi_v - \sin(\omega t + \frac{\pi}{2})\sin\psi_v]$$

$$= |R_v|\left(\frac{\hat{u}}{\bar{a}}\right)^{(i)} [-\cos\psi_v \sin\omega t - \sin\psi_v \cos\omega t] \tag{15}$$

The parts of equations (14) and (15) which are proportional to cos ωt and therefore can be in phase with the pressure oscillation are:

$$\left(\frac{\hat{r}}{\bar{a}}\right)_p^{(r)} = |R_b| \cos\psi_b \frac{\hat{p}}{\bar{p}} = R_b^{(r)} \frac{\hat{p}}{\bar{p}} \tag{16}$$

$$\left(\frac{\hat{r}}{\bar{a}}\right)_{(v)}^{(r)} = -|R_v| \sin\psi_v \left(\frac{\hat{u}}{\bar{a}}\right)^{(i)} = -R_v^{(i)} \left(\frac{\hat{u}}{\bar{a}}\right)^{(i)} \tag{17}$$

Note that according to equation (9), $(\hat{u}/\bar{a})^{(i)}$ has a negative sign, $(\hat{u}/\bar{a})^{(i)} = -(\varepsilon/\gamma)\sin(\pi z/L)$.

What these results show is that for pressure coupling, it is the real part of the response function which controls the destabilizing tendency and for velocity coupling it is the imaginary part.

It must be emphasized that the phase of the pressure-coupled response function is that for the oscillatory burning rate with respect to the pressure, but the phase ψ_v of the velocity-coupled response function is for the burning rate with respect to the velocity fluctuation. The reason that the imaginary part of R_v is required to specify the destabilizing tendency of velocity coupling is that the acoustics introduces a $\pi/2$ phase difference between the velocity and pressure oscillations, as shown by equation (5). Thus, an additional phase difference, provided by the response function R_v, is required to produce a component of the burning rate which may be in phase with the pressure. Only in this way is the principle cited earlier satisfied.

Choosing the parts of $(r'/\bar{r})_p$ and $(r'/\bar{r})_v$ which vary as cos ωt serves to eliminate those portions which cannot affect the stability of pressure waves. According to the principle stated on page 7, the fluctuations of burning rate must be in phase with $\hat{p}/\bar{p}$ to be destabilizing tendencies. This is a statement about the sign of r', namely that $\hat{r}^{(r)}/\hat{p}$ must be positive for instability. Thus, in order that the contributions represented by equations (16) and (17) cause instability:

$$\frac{(\hat{r}/\bar{r})_b^{(r)}}{\hat{p}/\bar{p}} = R_b^{(r)} > 0 \tag{18}$$

$$\frac{(\hat{r}/\bar{r})_v^{(r)}}{\hat{p}/\bar{p}} = -R_v^{(i)} \frac{(\hat{u}/\bar{a})^{(i)}}{\hat{p}/\bar{p}} > 0 \tag{19}$$

Note that for quasi-steady behavior, the sign of $(\hat{r}/\bar{r})_v^{(r)}/(\hat{p}/\bar{p})$ is fixed by the slope of the steady burn rate graphed as a function of pressure or parallel velocity. For the examples shown in Figures 2 and 3, the contributions are destabilizing.

For pressure coupling to be an unstable influence, the general statement, according to equation (18), is that the real part of the pressure-coupled response function must be positive. This is true for

all frequencies for real propellants. If $R_b^{(r)} > 0$, all elements of burning surface everywhere in the chamber contribute destabilizing influences. For velocity coupling, with the four assumptions listed above, the product of the imaginary part of the velocity-coupled response times the ratio of the spacial parts of the velocity and pressure fluctuations must be positive to cause instability. The situation is more complicated than for pressure coupling, and two cases must be considered, distinguished by the sign of $R_v^{(i)}$.

$$R_v^{(i)} > 0$$

For velocity coupling to be destabilizing, the velocity fluctuation must have a component in phase with the pressure fluctuation, $\hat{u}/\hat{p} > 0$. Consider again the fundamental longitudinal mode, and Figure 5; $\hat{u}/\hat{p}$ is positive only in the head end of the chamber, $0 \leq z < L/2$. Thus, if the imaginary part of the velocity coupled response function is positive, the contribution from burning surface in the forward half is destabilizing and the contribution from the aft half is stabilizing. This conclusion follows directly from equation (19) upon substituting equations (7) and (8), giving

$$- R_v^{(i)} \frac{(\hat{u}/\bar{a})^{(i)}}{(\hat{p}/\bar{p})} = R_v^{(i)} \frac{\sin \frac{\pi z}{L}}{\gamma \cos \frac{\pi z}{L}} = \frac{1}{\gamma} R_v^{(i)} \tan \left(\frac{\pi z}{L}\right)$$

The tangent function is positive in the forward half of the chamber.

$$R_v^{(i)} < 0$$

Obviously the situation is the reverse of that for $R_v^{(i)} > 0$. The contribution from the forward half is stabilizing and the contribution from the aft half is destabilizing, for the fundamental mode.

The same sort of reasoning can be applied to the higher modes of the chamber. Suppose that the imaginary part of the velocity coupled response is positive, $R_v^{(i)} > 0$. The pressure fluctuation always has maximum amplitude, and the velocity fluctuation is zero, exactly at the head-end, for all modes. In a region near the head-end, the velocity lags the pressure by $\pi/2$. Thus, there is a length of propellant surface, starting at the head-end, which under the influence of velocity coupling, is destabilizing for all modes.

At the aft end of the chamber, the pressure fluctuation also has maximum amplitude; it is out of phase with the pressure at the head end for even modes and in phase for odd modes. The velocity fluctuation at the aft end leads the pressure by $\pi/2$ for some distance upstream of the end. There is, consequently, some portion of propellant surface, stretching from the aft end, which is stabilizing under the influence of velocity coupling. Regions of stabilizing and destabilizing influence alternate along the chamber, and can readily be identified by extension of the preceding argument. Figure 7 shows the situation for the third and fourth modes, with $R_v^{(i)} > 0$. To compress the information into single figures, the mode shapes of pressure and velocity, are shown as they occur for their respective maximum amplitudes, i.e., they are sketched for instants of time separated by one-quarter of a period (see Figure 5).

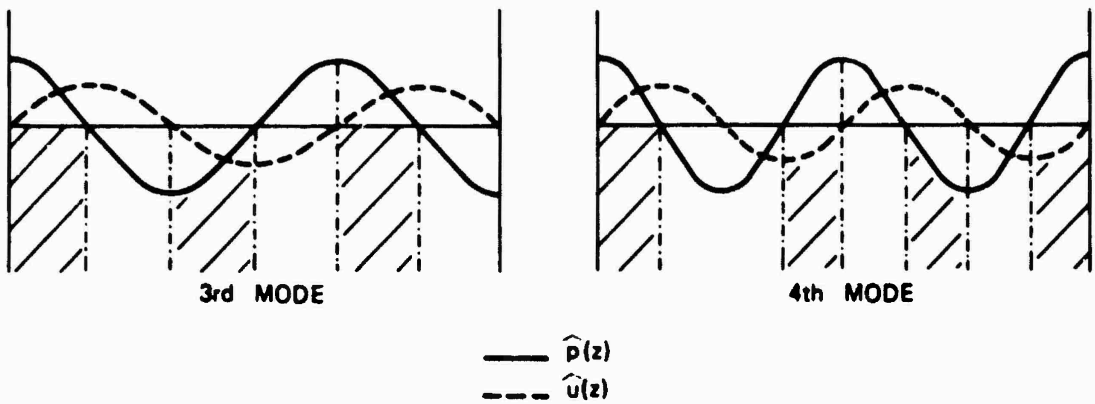

FIGURE 7. The Influence of Velocity Coupling for the Third and Fourth Longitudinal Modes.

So far in this discussion nothing has been assumed concerning the relationship between the response functions R_b and R_v. In practice, it is often supposed that R_v is proportional to R_b. This approximation is based on the ideas that processes in the gases respond in a quasi-steady fashion, if the frequencies of oscillation are not too high, and that the principal source of a time lag in the response is unsteady heat transfer in the solid phase. If we further assume that the response function R_b for pressure coupling is reasonably approximated by the familiar two parameter form,[4] then we are able to relate the sign of $R_v^{(i)}$ to the frequency of the mode considered. Figure 8 is a sketch of the real and imaginary parts of R_b, and therefore R_v, as functions of the dimensionless frequency $\Omega = \omega\kappa/r^2$.

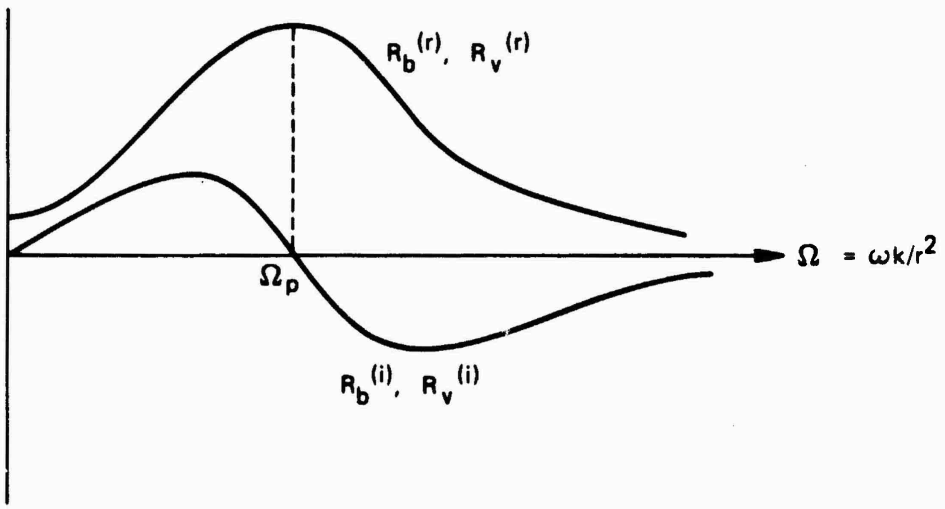

FIGURE 8. Real and Imaginary Parts of the Response Function.

The real part $R_b^{(r)}$ has a maximum at $\Omega = \Omega_\rho$ at which frequency, or nearly there, $R_b^{(i)}$ passes through zero. For frequencies less than $\bar{r}^2\Omega_p/\kappa$, the imaginary part of R_b, and therefore $R_v^{(i)}$ as well, is positive; this is the first case discussed above. Combined with the discussion of the first and second cases above, this completes the basis for the following statements often encountered, in one form or other, in the literature dealing with velocity coupling:

(1) In the low frequency range (i.e., $\omega < \bar{r}^2\Omega_p/\kappa$, the burning rate leads the pressure (i.e., $R_b^{(i)}$, $R_v^{(i)} > 0$) and velocity coupling in the forward half of the chamber is destabilizing for the fundamental mode.

(2) In the high frequency range ($\omega > \bar{r}^2\Omega_\rho/x$) the burning rate lags the pressure ($R_b^{(i)}$, $R_v^{(i)} > 0$) and velocity coupling in the aft half of the chamber is destabilizing for the fundamental mode.

An important aspect of velocity coupling which has so far been ignored in this discussion is rectification. The burning propellant should normally be sensitive to the magnitude of the parallel velocity, but not the direction. Suppose that an element of surface is exposed only to an oscillatory component of velocity having frequency ω,

$u' = \hat{u} \cos \omega t$. Then because the combustion processes should be sensitive to the magnitude but not the direction of parallel flow, the burning rate should be related to the magnitude of u':

$$|u'| = |\hat{u}| \cos \omega t \tag{20}$$

which is sketched in Figure 9.

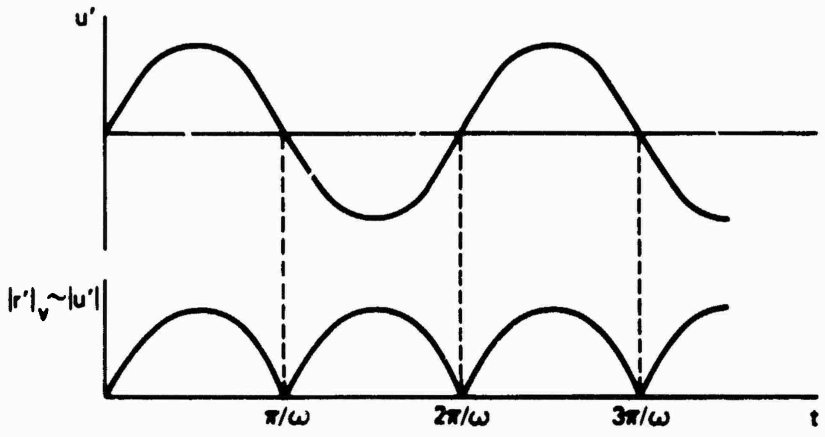

FIGURE 9. Rectification of a Velocity Oscillation.

The oscillatory part of $|u'|$, and therefore the burning rate responding to the parallel velocity, has frequency 2ω, not ω. Consequently, the input disturbance of frequency ω cannot be reinforced and velocity coupling cannot be acting in this case. This of course is due to the rectification noted above and shown in Figure 9. Note that rectification also produces a DC component which may be reflected as a change in steady erosive burning.

The phenomenon of rectification must always be present, but it does not preclude the possibility of having velocity coupling at the fundamental frequency ω. What is required is that the mean velocity in the same direction as the fluctuation be non-zero. The extreme case, sketched in Figure 10, occurs when $\bar{u} > u'$; there is then obviously a component of $|\bar{u} + u'|$ at the frequency ω, namely u' itself.

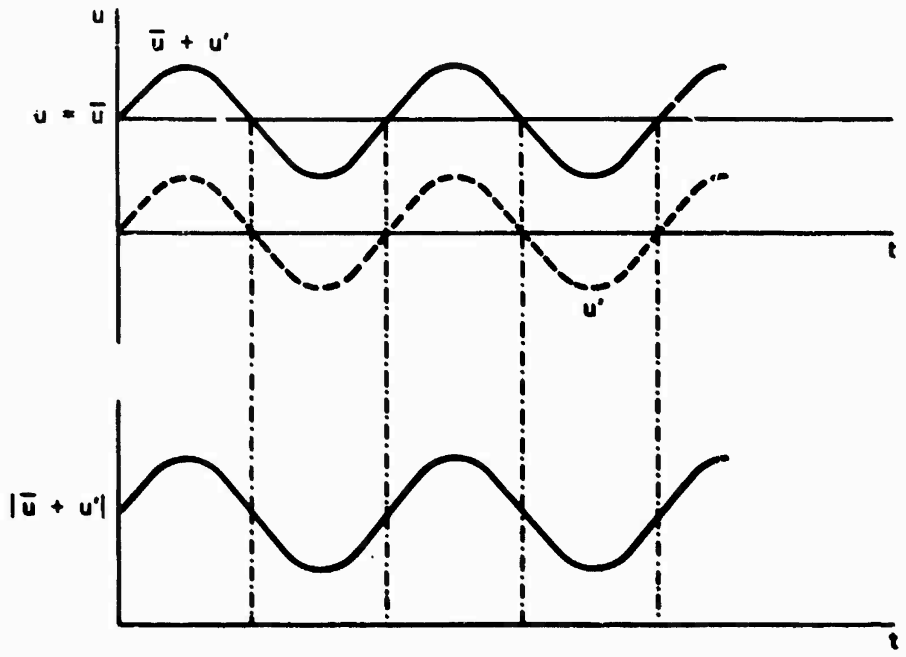

FIGURE 10. Rectification Prevented by Mean Flow.

If $0 < \bar{u} < |u'|$, the situation is somewhat more complicated, as shown by Figure 11. The part of $|\bar{u} + u'|$ which has the freqeuncy ω of u' must be found by Fourier decomposition of $|\bar{u} + u|$. Because the results depend on the amplitude of u', rectification introduces nonlinear behavior. Note that this is a consequence of the kinematics and the assumption that the response of the burning surface is sensitive to the direction but not the magnitude of the velocity; this has nothing whatever to do with the details of the combustion processes.

Now the average velocity $\bar{u}$ varies along the chamber, in general increasing with distance from the head end, so that the amplitude of that part of $|\bar{u} + u'|$ having frequency ω also varies along the chamber. The earlier discussion remains valid if the definition of R_v is assumed to include the influence of rectification. That is, there is an implied multiplicative factor proportional to the Fourier coefficient associated with that component of $|\bar{u} + u'|$ having the frequency of the mode being considered.[2 3 5] This has the important consequence that the function R_v is a strong function of position along the axis of the chamber, generally having greatest magnitude in the aft portion of the chamber where the mean flow speed is larger. Thus one should anticipate that the influence of velocity coupling is in some sense more sensitive to changes in the aft end of the chamber.

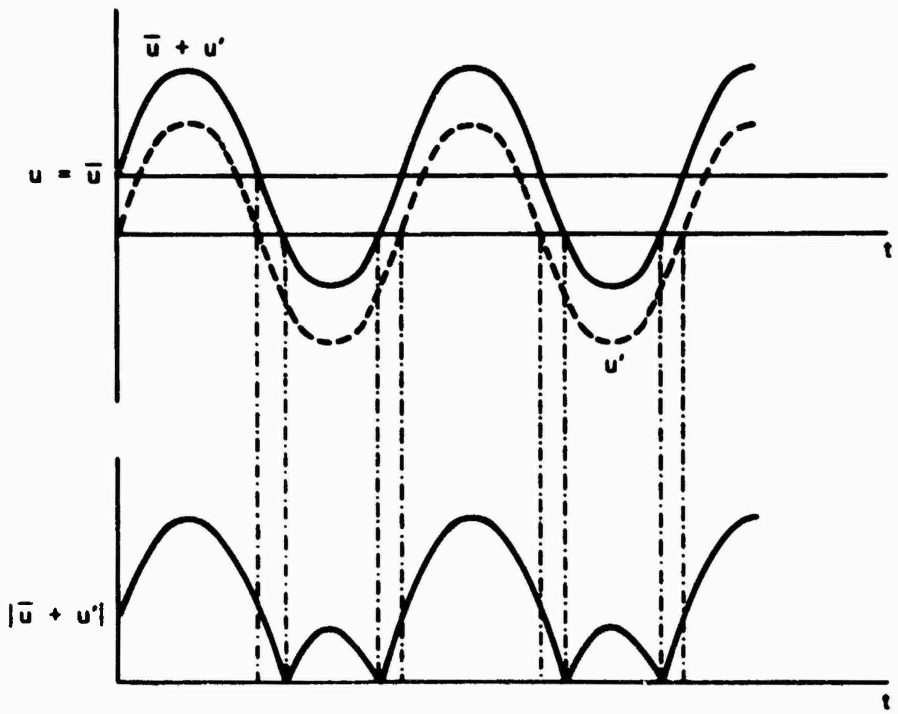

FIGURE 11. Partial Rectification in the Presence of Mean Flow.

For example, assume that the dependence of the velocity-coupled response function on frequency is that shown in Figure 8. Suppose that the burning rate and geometry are such that the dimensionless frequency Ω is less than Ω_p. The influence of velocity coupling in the forward half of the chamber is destabilizing for the first mode. But this is weak because of the weakness of rectification over the forward portion of the grain. Now suppose that the burning rate is decreased so that $\Omega > \Omega_p$, so that velocity coupling in the aft end where rectification is stronger, is destabilizing. Such a change of burning rate may be accompanied by a sufficient increase in the influence of velocity coupling, as to cause an initially stable fundamental mode to become unstable.

These remarks serve to emphasize that the influence of velocity coupling is intrinsically dependent on position in the chamber. It is true that the most basic piece of information is the imaginary part of the velocity-coupled response function, such as sketched in Figure 8. This should ideally be known as a function of dimensionless frequency, without the influence of rectification. To obtain a quantitative assessment of the stability of wave motions in a chamber with velocity coupling, a much more elaborate analytical structure is required to account for spacial variations in the chamber. That is the subject of the following section.

2. STABILITY ANALYSIS WITH VELOCITY COUPLING

In the preceding section, the answer to the question of stability rested ultimately on the principal stated earlier. However reasonable that proposition may seem--and it should be at least appealing, because it is true--nevertheless it was simply stated without proof. The formal analysis outlined in the following paragraphs will produce an explicit statement of the principle, and in such a form that it can be used to obtain quantitative results for practical situations. It is not the purpose here to provide a detailed exposition of the analysis, but rather to review the salient features. First the linear stability analysis will be covered and then, for future reference, an approximate nonlinear analysis will be summarized.

2.1 FORMULATION OF LINEAR STABILITY ANALYSIS

The most recent treatment of linear stability analysis, essentially the form used in all current computer codes, appeared as Reference 6. A treatment of velocity coupling, using essentially the same analytical framework, appeared earlier in Reference 7. The idea on which the analyses are based is that, for linear behavior, any arbitrary disturbance in a chamber may be represented by Fourier analysis as a superposition of contributions from all of the normal modes of the chamber. If one of the modes should be unstable, i.e., grow in time, then so is the disturbance. Hence, the stability of an arbitrary disturbance may be determined by finding the stability of all the normal modes of the chamber. By definition, a normal mode of a linear system varies harmonically in time, and the study of general linear stability comes down to studying the behavior of harmonic oscillations.

Thus, the time dependence $\exp(i\omega t)$ is assumed, with ω real if the oscillation neither grows nor decays in time. In order to display more clearly the contributions to the stability of motions, it is more convenient to calculate the growth or decay constant α, defined by assuming the complex exponential dependence $\exp(i(\omega-i\alpha)t) = \exp(i\omega t)\exp(\alpha t)$. If α is positive, the motion is unstable; processes which cause α to be positive are said to be destabilizing. The combination $k = (\omega-i\alpha)/\bar{a}$, where $\bar{a}$ is the speed of propagation of small disturbances, is the complex wave number. All analyses of the linear stability for combustion chambers lead eventually to results for k.

The general analysis is based on the equations of conservation for the flow in the chamber. Although the procedure is a bit tedious, it can be summarized as a sequence of several steps which are important to recognize. This is a simple way of emphasizing the important approximations.

First, in a more general vein, the formulation of the problem begins with the notion that the behavior of waves in a combustion chamber is a consequence of relatively small influences. The idea is that the structure (spatial distribution and time dependence) of a normal mode for the real problem, including combustion and flow, is "nearly" that for a classical acoustic mode in a chamber having the same geometry, but with no combustion and flow. If the frequency of the nth classical mode is ω_n, then the constant α, and the change of frequency $\omega-\omega_n$ for the corresponding mode in the combustion chamber, are small compared with ω_n:

$$\alpha, \omega - \omega_n \ll \omega_n \tag{21}$$

It is not assured a priori that this inequality is true, but it has been verified both analytically and experimentally for most situations encountered in practice.

It follows from this approximation and the assumption of linear behavior that there are two small quantities characterizing the general problem: the amplitude of the motions, and a measure of the perturbations due to combustion and average flow. These are, respectively, the Mach number M'_o for the amplitude of the fluctuation, and a Mach number $\bar{M}_o$ representative of the average flow field. Construction of a suitable set of differential equations rests on a formal limit process defined by the relative sizes of M'_o and $\bar{M}_o$. If $\bar{M}_o = 0$ and $M'_o \to 0$, all influences of combustion vanish, and classical linear acoustics is recovered. If $\bar{M}_o = 0$, and M'_o remains finite, equations for nonlinear classical acoustics are found.

The equations for linear acoustics with combustion and flow are defined by the limit process

$$M'_o \to 0, \bar{M}_o \ll 1; M'_o/\bar{M}_o \to 0 \tag{22}$$

This implies that the Mach numbers of both the acoustic and average flow fields must be small, but that for the acoustic field must be smaller. If $M_o \ll 1$ but is not allowed to go to zero, equations for nonlinear acoustics with combustion are obtained. The simplest nonlinear problems are defined by

$$M'_o \ll 1, \bar{M}_o \ll 1, M'_o/\bar{M}_o \sim O(1) \tag{23}$$

This limit process provides the basis for the approximate nonlinear analysis described in the following section.

It is important that the formal basis just described be recognized, although it is not necessary to be aware of all the details. The formulation of the problem eventually determines what input data are required for numerical computations.

With these preliminary remarks, we now describe briefly the procedure leading to a formula for the complex wavenumber.

1. The general conservation equations are written first for the mixture of gas and particles. Then the equations are split into two sets, one set for the gas phase and one for the particulate phase. This step defines the representations of interactions between the two phases: exchanges of mass, momentum (the drag force), and energy (heat transfer).

2. Earlier work on combustion instability was based essentially on the two sets of equations formed in step 1. However, for propellants heavily loaded with metal, this turns out to be a poor strategy. The speed of sound in the mixture may be 20% (or more) less than the value for that of the gas only. If the two sets of equations for the two phases are maintained separate, the change in the speed of sound is computed as part of the analysis. But the change is too large a perturbation to be handled accurately. Thus it is much more satisfactory to incorporate the influence of particle loading in the "zeroth order" problem by suitable combination of the two sets of equations; this procedure is described in Reference 6. The result is that the speed of sound in all that follows is the speed of propagation for small disturbances in the gas/particle mixture, denoted $\bar{a}$.

3. The equations are then linearized according to the process defined by equation (22). This produces a set of first order linear partial differential equations with source terms proportional to the Mach number of the average flow. (There are some contributions associated with gas/particle interactions which do not depend on the average flow, but are nevertheless small perturbations.) These equations can be combined to produce an inhomogeneous wave equation for the pressure field, and an associated inhomogeneous boundary condition for the normal component of the pressure gradient

$$\nabla^2 p' - \frac{1}{\bar{a}^2} \frac{\partial^2 p'}{\partial t^2} = h \tag{24}$$

$$\hat{n} \cdot \nabla p' = -f \tag{25}$$

The assumption of harmonic time dependence is now introduced to give the problem to be solved,

$$\nabla^2\hat{p} + k^2\hat{p} = \hat{h} \tag{26}$$

$$\hat{n} \cdot \nabla\hat{p} = -\hat{f} \tag{27}$$

At this stage, the wavenumber k is unrestricted--it is not identified with any particular mode.

4. Equation (26) with the boundary condition (27) can be solved by use of a Green's function, followed by an iteration procedure. However, to the order of small perturbations (linear in $\bar{M}_o$) usually treated, the following simple procedure gives the same result. The perturbations represented by $\hat{h}$ and $\hat{f}$ are necessarily small for this analysis to work well. Then the mode shape $\hat{p}$ and wavenumber k cannot be very different from the corresponding quantities ($\hat{p}_n$, k_n) for the classical acoustic mode in a closed chamber having the same shape. The unperturbed problem is described by the equations

$$\nabla^2\hat{p}_n + k_n^2\hat{p}_n = 0 \tag{28}$$

$$\hat{n} \cdot \nabla\hat{p}_n = 0 \tag{29}$$

In a certain sense, the "difference" between the perturbed and unperturbed problems contains the information we seek for the gains and losses of energy associated with the perturbations. This is contained in the formula for the wavenumber. The "difference" between the problems is formed by multiplying equation (26) by $\hat{p}_n$, equation (28) by $\hat{p}$, subtracting and integrating over the volume to give

$$\int[\hat{p}_n\nabla^2\hat{p} - \hat{p}\nabla^2\hat{p}_n]dV + (k^2 - k_n^2)\int \hat{p}\,\hat{p}_n dV = \int\hat{h}\hat{p}_n dV$$

The first volume integral can be integrated by parts by use of Green's theorem, with the boundary conditions (equation (27) and (29)) inserted, leading to:

$$\int[\hat{p}_n\nabla^2\hat{p} - \hat{p}\nabla^2\hat{p}_n]dV = \iint[\hat{p}_n\nabla\hat{p} - \hat{p}\nabla\hat{p}_n] \cdot \hat{n}\, dS = -\iint \hat{f}\,\hat{p}_n dS$$

in the second volume integral, $\hat{p} \cong \hat{p}_n$ for first order in small quantities, and the final result can be written

$$k^2 = k_n^2 + \frac{1}{\int \hat{p}_n^2 dV} \left\{ \int\int\int \hat{h}\, \hat{p}_n \, dV + \iint \hat{f}\, \hat{p}_n dS \right\} \tag{30}$$

This result is the basis for nearly all current analyses of linear stability in solid propellant rockets and will be used here to examine in greater detail the influence of linear velocity coupling.

The functions $\hat{h}$ and $\hat{f}$ are defined during the construction of the wave, equation (24), and its boundary condition. They contain representations of all processes contributing to the losses and gains of acoustic energy. Only one part will be examined here. It arises in the boundary condition expressing the fact that, owing to the response of the combustion processes, there are fluctuations of the flow inward at the surface. The origin of this term may be easily demonstrated. The linearized momentum equation has the form:

$$\bar{\rho} \frac{\partial u'}{\partial t} = \nabla p' + \ldots$$

For harmonic motions, the gradient of the pressure normal to the surface is:

$$\hat{n} \cdot \nabla \hat{p} = -i\bar{\rho}\bar{a}k\hat{u} \cdot \hat{n} \tag{31}$$

Actually, there is another contribution, a combination of part of $\hat{h}$ and part of $\hat{f}$, which must also be included, to give the formula for k^2:

$$k^2 = k_n^2 - \frac{i\bar{\rho}\bar{a}k_n}{\int \hat{p}_n^2 dV} \iint \left[\hat{u}\, \hat{p}_n + \bar{u} \frac{\hat{p}_n^2}{\bar{\rho}\bar{u}^2}\right] \cdot \hat{n} dS \tag{32}$$

The sign has been changed so that while $\hat{n}$ is still the outward normal, both $\hat{u}$ and $\hat{u} \cdot \hat{n}$ are positive inward. It is often useful to express

this result in terms of the mass flow; from equation (31) of Reference 6,

$$\hat{\vec{u}} \cdot \hat{n} + \hat{\vec{u}} \cdot \hat{n} \frac{\hat{p}}{\bar{\rho}\bar{a}^2} = \frac{1 + C_m}{\bar{\rho}} (\hat{m}_b + \bar{m}_b \frac{\hat{\Delta T}}{\bar{T}}) \tag{33}$$

The particulate loading ($\bar{\rho}_c/\bar{\rho}$), the mass of particles per volume of chamber) is C_m, and ΔT is the difference between the fluctuations of temperature at the edge of the combustion zone and in the acoustic field in the flow outside the combustion zone. For subsequent discussion we shall ignore the temperature differences and the influence of particles, so $\hat{\Delta T} = C_m = 0$. Hence, equations (32) and (33) lead to:

$$k^2 = k_n^2 - \frac{i\bar{a}k_n}{\int \hat{p}_n^2 dV} \iint \hat{m}_b \hat{p}_n dS \tag{34}$$

In the first section, equations (12) and (13), the response functions were introduced and related to fluctuations of the linear burning rate. What appears in equation (34) is the fluctuation of mass flux departing the combustion zone and entering the chamber. If one accepts the assumption of quasi-steady behavior in the gas phase

$$m_b' = \rho_c r' \quad \text{and} \quad \hat{m}_b = \rho_c \hat{r} \tag{35}$$

where ρ_c is the density of the unburned solid propellant. Hence

$$\frac{\hat{m}_b}{m_b} = \frac{\hat{r}}{r} \tag{36}$$

and the two response functions may be defined as

$$R_b = \frac{m_b'/\bar{m}_b}{p'/\bar{p}} = \frac{\hat{m}_b/\bar{m}_b}{\hat{p}/\bar{p}} \quad ; \quad R_v = \frac{m_b'/\bar{m}_b}{(u'/\bar{a})_v}$$

Here $(u'/\bar{a})_v$ represents an effective velocity fluctuation, parallel to the surface, which approximately accounts for rectification and the

threshold velocity; see Figures 9 through 11 and the accompanying discussion in the previous section. Because the analysis described here is linear, the correct nonlinear influences of rectification and threshold velocity cannot be rigorously accommodated without further discussion. These nonlinear effects will be properly treated in the following section.

For the sake of the argument here, we assume that pressure and velocity coupling are linearly additive, so that substitution of the definitions of equation (37) into equation (34) gives:

$$k^2 = k_n^2 - i\,\frac{\gamma \bar{m}_b}{\bar{\rho}\bar{a}}\,\frac{\bar{p}^2 k_n}{\int \hat{p}_n^2 dV}\left\{c_b \iint R_b\left(\frac{\hat{p}_n}{\bar{p}}\right)^2 dS + c_v \left[\widehat{R_v\left(\frac{u'}{\bar{a}}\right)}_v\right]\frac{\hat{p}_n}{\bar{p}}\,dS\right\} \quad (38)$$

where c_b, c_v are real constants whose values are unspecified. They simply express the relative weighting of pressure and velocity coupling. It is to be noted that $\hat{p}/\bar{p}$ in equation (37), the actual pressure fluctuation has been replaced by $(\hat{p}_n/\bar{p})$, the unperturbed mode shape. This is justified in the previous discussion of the linearization of equations of motion. Because $\hat{m}_b/\bar{m}_b$ is first order in small quantities, retention of $\hat{p}/\bar{p}$ instead of $\hat{p}_n/\bar{p}$ in equations (37) and (38) add terms of second and higher order which must be dropped.

Special attention must be paid to the integrand of the second integral in equation (38). The circumflex (^) over the term $R_v(u'/\bar{a})_v$ means that the exponential time dependance exp(iωt) must be removed. Because $(u'/\bar{a})_v$ is nonlinear when rectification is accounted for, this requires careful interpretation explained below following equation (54).

Now k is complex, $k = (\omega - i\alpha)/\bar{a}$, and its square is:

$$k^2 = \frac{1}{\bar{a}^2}(\omega^2 - \alpha^2) - i\left(2\,\frac{\alpha\omega}{\bar{a}}\right) \quad (39)$$

The bracketed terms in equation (38) are corrections of first order in the Mach number of the average flow. Consequently, both α and the change of frequency, $\omega - \omega_n$, are first order, and again because higher order terms must be dropped, equation (39) must be approximated by:

$$k^2 = \frac{\omega^2}{\bar{a}^2} - i\left(2\,\frac{\alpha\omega_n}{\bar{a}^2}\right) \quad (40)$$

With $k_n = \omega_n/\bar{a}$, the real and imaginary parts of equation (38) are:

$$\omega^2 = \omega_n^2 + \omega_n \frac{\bar{\gamma m}_b}{\bar{\rho}} \frac{\bar{p}^2}{\int \hat{p}_n^2 dV} \left\{ c_b \iint R_b^{(i)} \left(\frac{\hat{p}_n}{\bar{p}}\right)^2 dS + c_v \iint \left[R_v \left(\frac{u'}{\bar{a}}\right)_v \right]^{(i)} \frac{\hat{p}_n}{\bar{p}} dS \right\} \quad (41)$$

$$\alpha = \frac{1}{2} \frac{\bar{\gamma m}_b}{\bar{\rho}} \frac{\bar{p}^2}{\int \hat{p}_n^2 dV} \left\{ c_b \quad R_b^{(r)} \frac{\hat{p}_n}{\bar{p}}^2 dS + c_v \iint \left[R_v \left(\frac{u'}{\bar{a}}\right)_v \right]^{(r)} \left(\frac{\hat{p}_n}{\bar{p}}\right) dS \right\} \quad (42)$$

The meanings of the real and imaginary parts of the integrands in the second integrals are explained below.

2.2 RAYLEIGH'S CRITERION DERIVED FROM LINEAR STABILITY ANALYSIS

Before proceeding further with equation (42), it is instructive to examine the interpretation of α, in particular its relation to "Rayleigh's criterion." According to the definition of k, the dependence of the pressure on time is:

$$\frac{p'}{\bar{p}} = e^{i\bar{a}kt} = e^{i(\omega - i\alpha)t} = e^{\alpha t} e^{i\omega t} \quad (43)$$

Hence, if α is positive, the fluctuation is unstable and grows exponentially with time. The time averaged acoustic energy $\langle \mathcal{E} \rangle$ is proportional to the time average of the real part of $(p')^2$, so:

$$\langle \mathcal{E} \rangle \sim e^{2\alpha t}$$

Differentiate with respect to time to produce the useful relation for α

$$\alpha = \frac{1}{2} \frac{1}{\langle \mathcal{E} \rangle} \frac{\langle \mathcal{E} \rangle}{dt} \quad (44)$$

In equation (42), the denominator, $\int \hat{p}_n^2 \, dV$, is proportional to $\langle \mathcal{E} \rangle$ and the numerator therefore represents the rate of increase of time-averaged acoustic energy in the chamber. This is the origin of the statement that α represents the difference between "gains" and "losses"

of acoustic energy. All processes contributing to the stability, or instability, of waves, may be interpreted in terms of their influences on the rate of change of acoustic energy in the chamber.

The criterion formulated by Rayleigh may be found on Page 226 of Reference 8.

> "If heat be given to the air at the moment of greatest condensation, or taken from it at the moment of greatest rarefaction, the vibration is encouraged."

The idea is that for greatest driving of the waves--maximum tendency towards instability--heat addition must occur in phase with the pressure wave and in the vicinity of a pressure anti-node. This conclusion may be deduced directly from equation (30). If distributed heat addition, Q (Energy/vol.-sec), is included in the equation for conservation of energy, it eventually contributes the following term to h' (equation (46) of Reference 6):

$$(h')_{\text{heat addition}} = -\frac{1}{\bar{a}^2}\left(\frac{\gamma - 1}{\gamma}\right)\frac{\partial Q'}{\partial t} \tag{45}$$

For harmonic motions,

$$(\hat{h})_{\text{heat addition}} = -i\,\frac{k_n}{\bar{a}}\left(\frac{\gamma - 1}{\gamma}\right)\hat{Q} \tag{46}$$

According to equation (30), the corresponding part of k^2 is

$$k^2 = k_n^2 - i\,\frac{k_n/\bar{a}}{\int \hat{p}_n^2 dV}\left(\frac{\gamma - 1}{\gamma}\right)\int \hat{Q}\hat{p}_n dV \tag{47}$$

The real and imaginary parts are

$$\omega^2 = \omega_n^2 + \frac{\omega_n}{\int \hat{p}_n^2 dV}\left(\frac{\gamma - 1}{\gamma}\right)\int \hat{Q}^{(i)}\hat{p}_n dV \tag{48}$$

$$\alpha = \frac{1}{2}\,\frac{1}{\int \hat{p}_n^2 dV}\left(\frac{\gamma - 1}{\gamma}\right)\int \hat{Q}^{(r)}\,\hat{p}_n dV \tag{49}$$

For a given mode, α is increased if the product $\hat{Q}^{(r)}\hat{p}_n$ is increased. This depends only on the real part of $\hat{Q}$, the part of the fluctuating heat addition which is in phase with the pressure fluctuation and $\hat{Q}^{(r)}\hat{p}_n$ is obviously greater if the heat addition occurs where the pressure is greater, i.e., at the anti-nodes.

Thus, Rayleigh's criterion and the general principle cited in the first section are both contained in the same analysis. These are merely two ways of expressing the transfer of energy required to drive and sustain acoustic waves.

2.3 RECTIFICATION AND THE EFFECTIVE VELOCITY

The formula (42) is the general representation for the coupling between surface combustion processes and acoustic waves. It is the precise representation of the discussion given in the introduction. As argued earlier and as shown in equation (42), it is the real part of the response function for pressure coupling which determines the tendency for instability due to pressure coupling. The second term in equation (42) contains the real part of the product of the response function for velocity coupling and the effective velocity.

Because of the way in which the analysis is constructed, the response function and the velocity fluctuation $(\hat{u}/\bar{a})_v$ are independent. Moreover, according to equation (9) $(\hat{u}/\bar{a})_v$ contains only a part which is out of phase with $p_n'/\bar{p}$. Hence, for use in equation (42),

$$\left[R_v\left(\frac{\hat{u}}{\bar{a}}\right)\right]^{(r)} = -R_v^{(i)}\left(\frac{\hat{u}}{\bar{a}}\right)_v^{(i)} \tag{50}$$

as shown earlier by equation (17). The difference between (17) and (50) is that the subscript $(\ )_v$ on $(\hat{u}/\bar{a})_v$ indicates that rectification and a threshold velocity are to be accounted for. This demonstrates once again that for velocity coupling it is the imaginary part of the response function which controls the tendency for instability.

According to equation (50), treatment of linear stability associated with velocity coupling comes down to two problems: analysis or measurement of the imaginary part of the response function; and determination of the effective velocity $(\hat{u}/\bar{a})_v$. The second problem is essentially a matter of kinematics which has been treated in several places, e.g., References 1 through 3 and 9 through 11. Little attention will be given here to efforts to calculate the response function itself. The intent is primarily to provide the basis for interpreting data. For this purpose, the effective velocity must be known.

What is required is the imaginary part of $(\hat{u}/\bar{a})_v$, that part which is out of phase with the pressure fluctuation. Consider again the simplest case of the fundamental longitudinal mode in a straight chamber. Either the real or the imaginary part of the complex pressure field may be used, and to be definite we use the real part of equation (2):

$$\frac{p'}{\bar{p}} = \varepsilon \cos \frac{\pi z}{L} \cos \omega_1 t \tag{51}$$

The corresponding velocity, parallel to the lateral surface is (5):

$$u' = \varepsilon \frac{\bar{a}}{\gamma} \sin \frac{\pi z}{L} \sin \omega_1 t \tag{52}$$

which is entirely out of phase with the pressure; the frequency is of course $\omega_1 = \bar{a}k = a/2L$ for the fundamental longitudinal mode.

The effective velocity must include the influence of rectification and the fact that these may be a threshold velocity. We shall list here the various possible cases, but the details will be worked out only for the case when the threshold velocity vanishes.

Three velocities are important: the average flow speed, $\bar{u}$, the acoustic velocity, u', and the threshold velocity u_t. We assume that the average flow is from left to right, $\bar{u}$ then being positive always; the threshold velocity is, by definition positive. In steady flow, erosive burning is supposed to occur whenever the average speed, $\bar{u}$, exceeds the threshold velocity. For unsteady motions we assume that erosive burning occurs whenever the resultant velocity $\bar{u} + u'$ exceeds u_t for motion to the right and when $-(\bar{u} + u')$ is greater than u_t for motion to the left. This becomes clearer from the diagrams given below.

What we call velocity coupling occurs when the erosive burning at any time during unsteady motions exceeds the erosive burning which would take place under the average conditions existing at the same time. The circumstances when there is no threshold velocity are most readily understood. There are then two possibilities: the magnitude of the acoustic velocity, $|u'|$, is either greater or less than the average velocity. These cases are sketched in Figure 12. The shaded areas denote the velocity effective in causing erosive burning under unsteady conditions. Note that rectification occurs whenever the resultant velocity, $\bar{u} + u'$, becomes negative, or the total effective velocity is $|\bar{u} + u'|$.

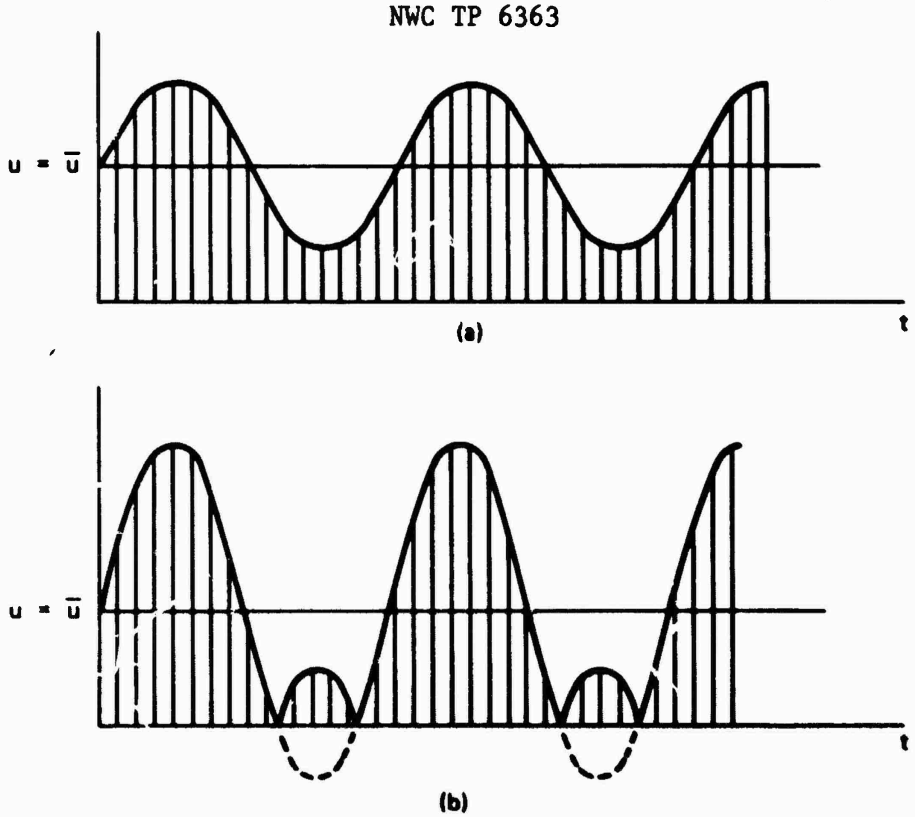

FIGURE 12. The Effective Velocity Due to Rectification.

Steady erosive burning is proportional to $\bar{u}$ itself, so the effective velocity for velocity coupling, when there is no threshold velocity, is

$$\left(\frac{u'}{\bar{a}}\right)_v = \frac{1}{\bar{a}} \left[|\bar{u} + u'| - \bar{u} \right] \tag{53}$$

Before considering the more complicated case of $u_t \neq 0$, let us work out the consequences of our discussion so far, to see how the results fit into the analysis of stability. According to equation (50) and earlier remarks, we need that part of equation (53) which oscillates out of phase with the pressure fluctuation but at the same frequency. To find that contribution, the formula (52) is used for u' and (53) is expanded in Fourier series,

$$\left(\frac{u'}{\bar{a}}\right)_v = C_o + \sum_{n=1}^{\infty} C_n \cos(n\omega_1 t) + \sum_{n=1}^{\infty} S_n \sin(n\omega_1 t) \tag{54}$$

For use in the formulas (41) and (42) we need only the terms which oscillate with frequency ω_1:

$$\left(\frac{u'}{a}\right)_v = C_1 \cos \omega_1 t + S_1 \sin \omega_1 t$$

To see what is required in (41) and (42) and to make the connection with the use of the complex notation, write this as the real part of the comlex function

$$\left(\frac{u'}{a}\right)_v = C_1 e^{i\omega_1 t} + S_1 e^{i(\omega_1 t - \pi/2)} = (C_1 - iS_1)e^{i\omega_1 t}$$

Then in (41) and (42), we can write

$$R_v\left(\frac{u'}{a}\right)_v = (R_v^{(r)} + iR_v^{(i)})(C_1 - iS_1)e^{i\omega_1 t}$$

$$= (R_v^{(r)} C_1 + R_v^{(i)} S_1) + i(R_v^{(i)} C_1 - R_v^{(r)} S_1)e^{i\omega_1 t}$$

Hence we find

$$\left[R_v \left(\frac{u'}{a}\right)_v\right]^{(r)} = R_v^{(r)} C_1 + R_v^{(i)} S_1$$

$$\left[R_v \left(\frac{u'}{a}\right)_v\right]^{(i)} = R_v^{(i)} C_1 - R_v^{(r)} S_1 \qquad (55)a, b$$

It is easy to show that the result (55)b reduces to the special case (50) when u' is the classical acoustic velocity. The complex form of $u'/\bar{a}$ is then given by (8),

$$\frac{u'}{\bar{a}} = \frac{\varepsilon}{\gamma} \sin(\pi\frac{3}{L}) e^{i(\omega_1 t - \frac{\pi}{2})}$$

and

$$R_v\left(\frac{u'}{\bar{a}}\right) = (R_v^{(r)} + iR_v^{(i)} \frac{\varepsilon}{\gamma} \sin(\pi\frac{z}{L})(-i)e^{i\omega_1 t}$$

$$= \frac{\varepsilon}{\gamma} \sin(\pi\frac{z}{L})(R_v^{(i)} - iR_v^{(r)})e^{i\omega_1 t}$$

Hence, corresponding to (55)a, b, we have

$$\widehat{\left[R_v\left(\frac{u'}{\bar{a}}\right)\right]}^{(r)} = R_v^{(i)} \frac{\varepsilon}{\gamma} \sin(\pi\frac{z}{L})$$

$$\widehat{\left[R_v\left(\frac{u'}{\bar{a}}\right)\right]}^{(i)} = -R_v^{(r)} \frac{\varepsilon}{\gamma} \sin(\pi\frac{z}{L})$$

The first of these is exactly (50) because $-\hat{u}/\bar{a}_v^{(i)} = (\varepsilon/\gamma) \sin(\pi z/L)$ from equation (9).

Although only the values of A_1 and B_1 are required here, we shall evaluate all the coefficients in (54). The forumulas for the coefficients are:

$$C_o = \frac{1}{2\pi} \int_o^{2\pi} \left(\frac{u'}{\bar{a}}\right)_v d(\omega_1 t)$$

$$C_n = \frac{1}{2\pi} \int_o^{2\pi} \left(\frac{u'}{\bar{a}}\right)_v \cos(n\omega_1 t)\, d(\omega_1 t) \qquad (56)a,b,c$$

$$S_n = \frac{1}{\pi} \int_o^{\pi} \left(\frac{u'}{\bar{a}}\right)_v \sin(n\omega_1 t)\, d(\omega_1 t)$$

The difficult part of evaluating the formulas arises from the term $|\bar{u} + u'|$ in (53), so this will first be treated separately. With (52), this factor may be written

$$\frac{1}{\bar{u}}\left(\bar{u} + u'\right) = 1 + \beta \sin \omega_1 t \tag{57}$$

where

$$\beta = \frac{\varepsilon \bar{a}}{\gamma \bar{u}} \sin \frac{\pi z}{L} \tag{58}$$

All possible cases will be covered by supposing first that $\beta > 1$. The function (58) appears as sketched in Figure 12(a) and expanded in Figure 13 for one cycle, $0 < \omega t < 2\pi$.

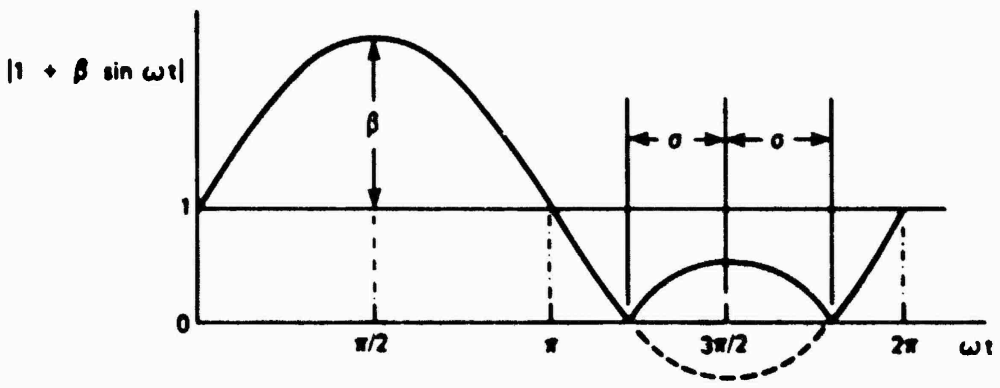

FIGURE 13. One Cycle of a Rectified Waveform for Mean Flow in the Positive Direction.

It is clear from the sketch that

$$|1 + \beta \sin \omega t| = (1 + \beta \sin \omega_1 t) \qquad 0 < \omega_1 t < \frac{3\pi}{2}$$

$$= -(1 + \beta \sin \omega_1 t) \qquad \frac{3\pi}{2} - \sigma < \omega_1 t < \frac{3\pi}{2} + \sigma$$

$$= (1 + \beta \sin \omega_1 t) \qquad \frac{3\pi}{2} - \sigma < \omega_1 t < 2\pi$$

The value of σ is set by the condition $1 + \beta \sin\left(\frac{3\pi}{2} + \sigma\right) = 0$, giving

$$\cos \sigma = \frac{1}{\beta} \qquad (\beta > 1) \tag{59}$$

For $\beta \leq 1$, there is no rectification, and $\sigma = 0$. With this representation, the following integrals may be found:

$$\frac{1}{2\pi}\int_0^{2\pi} |1 + \beta \sin \omega_1 t| d(\omega_1 t) = 1 - \frac{2}{\pi}\sigma + \frac{\beta}{\pi} \sin \sigma \tag{60}$$

$$\frac{1}{\pi}\int_0^{2\pi} |1 + \beta \sin \omega_1 t| \cos(n\omega_1 t) d(\omega_1 t)$$

$$= \begin{cases} -\frac{2}{\pi} \cos n\frac{\pi}{2}\left[\frac{2}{n} \sin n\sigma - \beta\left\{\frac{\sin/(n-1)\sigma}{(n-1)} + \frac{\sin(n+1)\sigma)}{(n+1)}\right\}\right] & (n \neq 1) \\ \frac{2}{\pi} \sin \sigma\left[1 - \frac{\beta}{2} \sin \sigma\right] & (n = 1) \end{cases} \tag{61}$$

$$\frac{1}{\pi}\int_0^{2\pi} 1 + \beta \sin \omega_1 t \sin(n\omega_1 t) d(\omega_1 t)$$

$$= \begin{cases} \frac{2}{\pi} \sin n\left(\frac{3\pi}{2}\right)\left[\frac{2}{n} \sin n\sigma + \beta\left\{\frac{\sin(n-1)\sigma}{n-1} - \frac{\sin(n+1)\sigma}{n+1}\right\}\right] & (n \neq 1) \\ \frac{4}{\pi} \sin \sigma + \beta\left[1 - \frac{2}{\pi}\sigma - \frac{1}{\pi} \sin 2\sigma\right] & (n = 1) \end{cases} \tag{62}$$

Values of these integrals for $\beta \leq 1$ (no rectification) follow directly upon setting $\sigma = 0$.

The integrals over $\bar{u}/\bar{a}$ in (56) contribute only to C_o, and the final results for no threshold velocity ($u_t = 0$) are

$$C_o = \frac{\bar{u}}{\bar{a}}\left[1 - \frac{2}{\pi}\sigma + \frac{2\beta}{\pi}\sin\sigma\right] - \bar{u} = \frac{\bar{u}}{\bar{a}}\frac{2}{\pi}[\beta\sin\sigma - \sigma] \tag{63}$$

$$C_1 = 0 \tag{64}$$

$$C_n = -\frac{\bar{u}}{\bar{a}}\frac{2}{\pi}\cos\left(n\frac{\pi}{2}\right)\left[\frac{2}{n}\sin n\sigma - \beta\left\{\frac{\sin(n-1)\sigma}{(n-1)} + \frac{\sin(n+1)\sigma}{(n+1)}\right\}\right] \tag{65}$$

$$S_1 = \frac{\bar{u}}{\bar{a}}\left[\frac{4}{\pi}\sin\sigma + \beta\left\{1 - \frac{2}{\pi}\sigma - \frac{1}{\pi}\sin 2\sigma\right\}\right] \tag{66}$$

$$S_n = -\frac{\bar{u}}{\bar{a}}\sin\left(n\frac{3\pi}{2}\right)\left[\frac{4}{n\pi}\sin n\sigma + \frac{2\beta}{\pi}\left\{\frac{\sin(n-1)\sigma}{(n-1)} - \frac{\sin(n+1)}{(n+1)}\right\}\right] \tag{67}$$

We have assumed here that only a simple sinusoidal oscillation, having frequency ω_1 is present in the chamber. This may be due to any mode. Because $C_1 = 0$, the driving of this mode itself, due to velocity coupling, is proportional to the coefficient S_1, as the remarks following (54) having shown. For use in (42), we therefore write

$$\left[\widehat{R_v\left(\frac{u'}{\bar{a}}\right)_v}\right]^{(r)} = \frac{\bar{u}}{\bar{a}}\left[\frac{4}{\pi}\sin\sigma + \beta\left\{1 - \frac{2}{\pi}\sigma - \frac{1}{\pi}\sin 2\sigma\right\}\right] \tag{68}$$

The other terms $S_n \cos(n\omega_1 t)$ in the series expansion (54) represent the influence of velocity coupling on harmonics of the mode having frequency ω. We shall see in the following section how these are incorporated in an approximate nonlinear analysis. Appendix A contains an application to T-burner data.

Now suppose one is concerned with the generation of a mode which has frequency ω_o not an integral multiple of the frequency ω_1. For example, one might suppose that a longitudinal mode may excite the transverse modes in a cylindrical chamber. For use in (42), one needs that part of $(\tilde{u}/\bar{a})_v$ which is proportional to $\cos\omega_o t$ with $\omega_o \neq \omega_1$. Because

we have assumed steady waves throughout, (54) may be used as a valid representation for all time, $-\infty < t < +\infty$. To find the contribution for any frequency, we may take the Fourier transform of (54) and extract the component having frequency ω_o. Define the transform pair

$$U(f) = \int_{-\infty}^{\infty} \left(\frac{u'}{\bar{a}}\right)_v e^{-i2\pi ft} dt \tag{69}$$

$$\left(\frac{u'}{\bar{a}}\right)_v = \int_{-\infty}^{\infty} U(f) e^{i2\pi ft} df \tag{70}$$

But after (57) is substituted into (65) and the integrals carried out, we find that U(f) consists of an infinite series of delta functions placed at $f = \pm\omega_1/2\pi$, $\pm 2\ \omega_1/2\pi$, $\pm 3\ \omega_1/2\pi$, $\ldots \pm n\omega_1/2\pi$. There is no component at the frequency ω_o. The reason for this, of course, is that $(u'/\bar{a})_v$ defined by (53) and expressed as (54) is periodic with frequency ω_1 and therefore has no component with frequency different from integral multiples of ω_1.

The important conclusion is: an unstable longitudinal mode will excite, due to velocity coupling, only longitudinal modes. The nonlinear behavior due to rectification can generate only integral harmonies of the primary mode. We must emphasize that the only nonlinearity accounted for here is rectification. Nonlinear behavior associated with the flow within the chamber may generate other modes, but the matter has not been studied.

When the threshold velocity is non-zero, the situation is considerably more complicated; a single calculation will not cover all possibilities. Rather than include the calculations here, we shall merely sketch the cases for information and to complete this discussion of the influences of rectification and threshold velocity.

It is convenient to classify the possibilities into two groups, those for which the average flow speed is greater than threshold and those for which the speed is less than threshold. First, for $\bar{u} > u_1$, there are three cases distinguished by the magnitude of the acoustic velocity. These are sketched in Figure 14. Again the velocity effective in causing erosive burning under unsteady conditions is shown by

the shaded regions. Note that there is not erosive burning if the resultant velocity $\bar{u} + u'$ does not exceed the value of the threshold velocity. Steady erosive burning is now proportional to $\bar{u} - u_t$, so the effective velocities for velocity coupling are given by the following formulas corresponding to Figure 14(a), (b) and (c):

(a) $\underline{|u'| < \bar{u} - u_t}$

$$\left(\frac{u'}{\bar{a}}\right)_v = [|\bar{u} + u'| - u_t] - (\bar{u} - u_t)$$

$$= |\bar{u} + u'| - \bar{u} \tag{71}$$

(b) $\underline{(\bar{u} - u_t) < |u'| < (\bar{u} + u_t)}$

$$\left(\frac{u'}{\bar{a}}\right)_v = 0 \qquad (-\bar{u}_t < \bar{u} + u' < u_t) \tag{72}$$

$$\left(\frac{u'}{\bar{a}}\right)_v = [|\bar{u} + u'| - u_t] - (\bar{u} - u_t)$$

$$= |\bar{u} + u'| - \bar{u} \qquad (\bar{u} + u' > u_t) \tag{73}$$

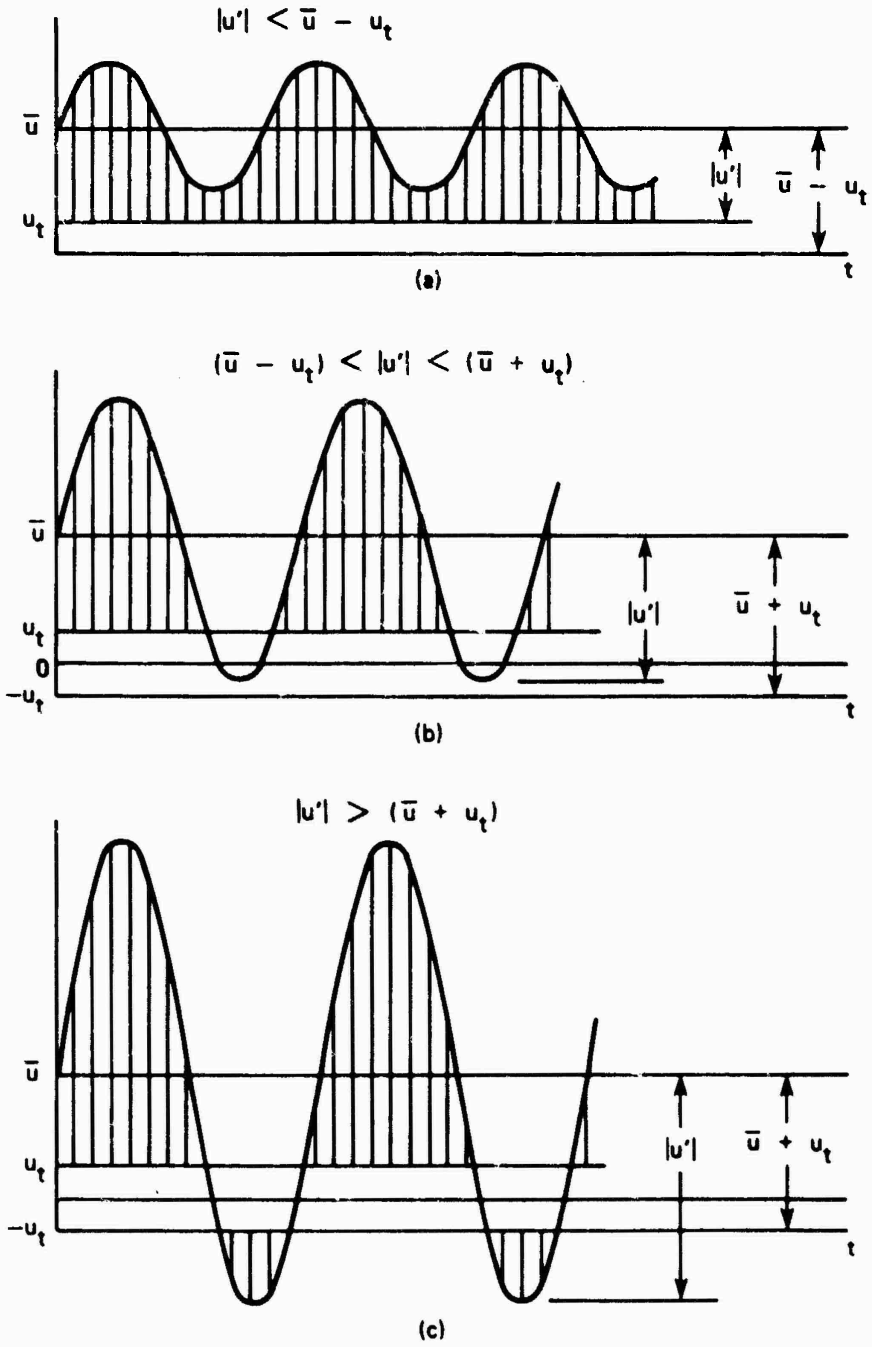

FIGURE 14. Rectified Waveforms When the Mean Velocity Exceeds the Threshold Velocity.

(c) $\underline{|u'| > (\bar{u} + u_t)}$

$$\left(\frac{u'}{\bar{a}}\right)_v = 0 \qquad (-u_t < \bar{u} + u' < u_t) \tag{74}$$

$$\left(\frac{u'}{\bar{a}}\right)_v = [|\bar{u} + u'| - \bar{u}_t] - (\bar{u} - u_t)$$

$$= |\bar{u} + u'| - \bar{u} \qquad (\bar{u} + u' > u_t) \tag{75}$$

$$\left(\frac{u'}{\bar{a}}\right)_v = [|\bar{u} + u'| - (\bar{u} + u_t)] - (\bar{u} - u_t)$$

$$= |\bar{u} + u'| - 2\bar{u} \qquad (\bar{u} + u' < -u_t) \tag{76}$$

The second group of possibilities arises when the mean-flow speed is less than the threshold velocity, $\bar{u} < u_t$. The three cases are sketched in Figure 15. Now the portions of each cycle during which erosive burning may occur are much smaller than for the previous cases. The formulas for the effective velocity coupling are

(a) $\underline{|u'| < u_t - \bar{u}}$

$$\left(\frac{u'}{\bar{a}}\right)_v = 0 \tag{77}$$

(b) $\underline{(u_t - \bar{u}) < u' < (\bar{u} + u_t)}$

$$\left(\frac{u'}{\bar{a}}\right)_v = 0 \qquad (\bar{u} + u' < u_t) \tag{78}$$

$$\left(\frac{u'}{\bar{a}}\right)_v = \bar{u} + u' - u_t \qquad (\bar{u} + u' > u_t) \tag{79}$$

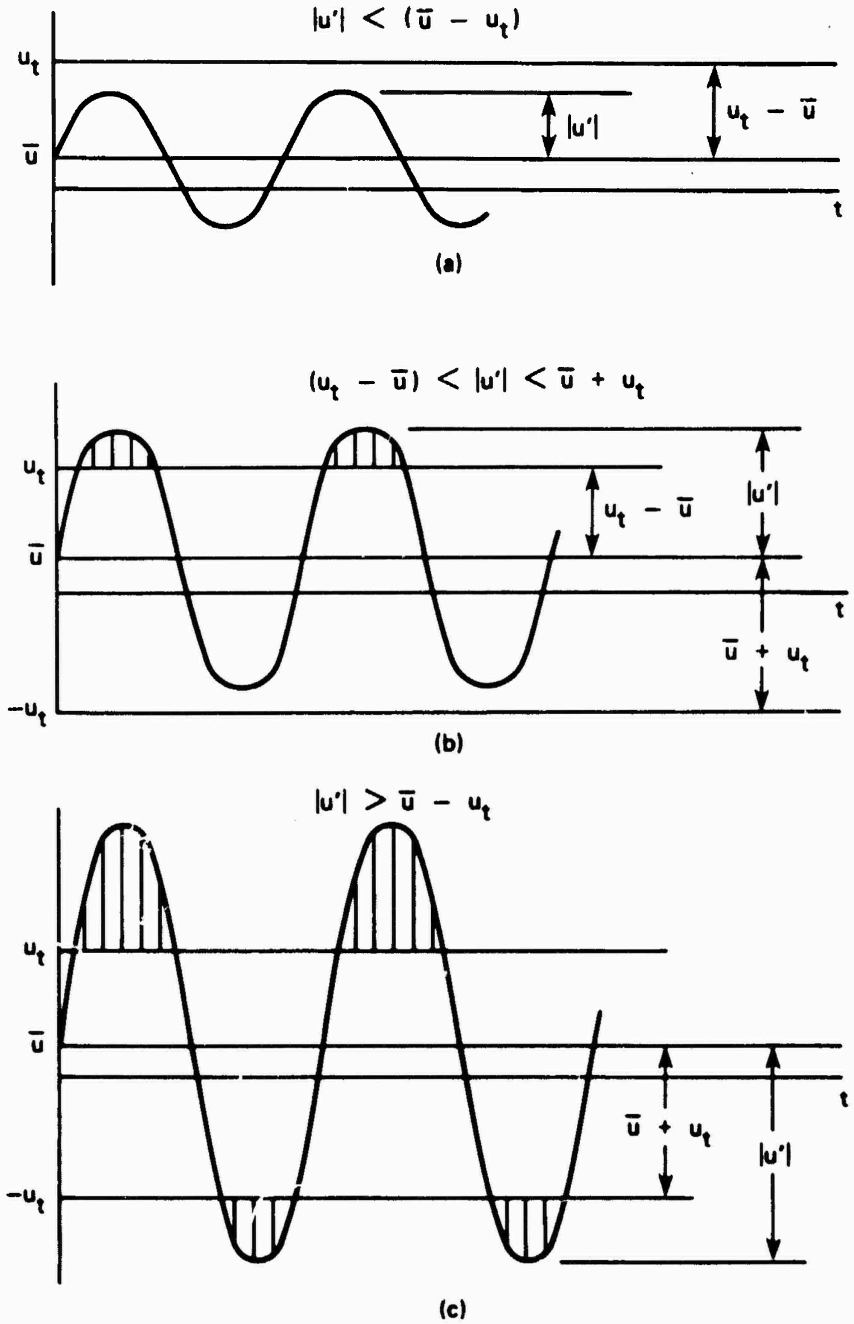

FIGURE 15. Rectified Waveforms When the Threshold Velocity Exceeds the Mean Velocity.

(c) $\underline{|u'| > (\bar{u} + u_t)}$

$$\left(\frac{u'}{\bar{a}}\right)_v = 0 \qquad (-u_t < \bar{u} + u' < u_t) \tag{80}$$

$$\left(\frac{u'}{\bar{a}}\right)_v = |\bar{u} + u'| - u_t \qquad (\bar{u} + u' > u_t) \tag{81}$$

$$\left(\frac{u'}{\bar{a}}\right)_v = |\bar{u} + u'| - (\bar{u} + u_t) \qquad (\bar{u} + u' < -u_t) \tag{82}$$

For use in the stability analysis the effective velocity must in these cases be analyzed into its components. Only the part proportional to sin ωt is required to determine the contribution to driving the fundamental mode. As an unstable wave grows, the conditions at a given position in the chamber (i.e., given $\bar{u}$ and u_t) progresses from case (a) in Figures 14 and 15 to case (c). And of course at a given location in the chamber, the relative values of the mean-flow speed and threshold velocity change. Hence, the appropriate formula for the effective velocity (equations (71) through (82)) changes with time. A correct analysis of stability therefore involves a considerable amount of bookkeeping. Some relevant numerical results have been given in Reference 5.

It is apparent from the preceding remarks that because of rectification, the growth constant, α, given by equation (42) with (68) used in the second term becomes a function of the amplitude $|u'|$ or $|p'|$ of the oscillations. Thus, what started as, and is strictly, a linear analysis of stability has apparently become a nonlinear analysis. The qualification "apparent" should be emphasized, however, because it is obvious from all of our previous discussions that no truly nonlinear analysis has been accomplished. The situation is better viewed at this point as characterized by a parameter (here the response function for velocity coupling) which changes with amplitude. A method for treating velocity coupling within a true nonlinear analysis is described in the next section.

In any case, it is certainly true that as a consequence of rectification it is quite possible that both the magnitude and the sign of the growth constant change with amplitude. A change of sign is especially interesting because it offers the opportunity for true nonlinear stability. It is possible that α is negative at low amplitudes but positive at high amplitudes. Under these circumstances a small amplitude wave is stable, but a large amplitude wave is unstable. An initially

small disturbance will therefore decay, but a sufficiently large disturbance will grow. This is an example of truly nonlinear unstability, sometimes called triggering.

Appeal has often made to the preceding reasoning to explain the dependence of instabilities on the amplitudes of pulses initiated in a motor. While the argument, or at least the essential idea, may be correct, there is no proof and not a single example which can be unambiguously explained on this basis. Indeed, there is in fact a serious lack of calculations which can be viewed simply as credible estimates of the phenomenon. There is an opportunity to carry out some useful calculations to provide a more systematic and quantitative basis for conclusions drawn, within the idealized framework described here.

To treat a nonlinear contribution correctly, it should be placed within a nonlinear analysis. Some "exact" numerical analysis has been done, e.g., Reference 11 and more recently Reference 12, with increasing success. Observed behavior has been reproduced qualitatively, and in some cases quantitatively, for nonlinear phenomena in solid rocket motors, although little has been done specifically to clarify velocity coupling. The calculations are expensive and restricted to one dimensional problems. Consequently, approximate analysis continues to be very attractive for many applications. One approach is summarized in the next section.

3. APPROXIMATE NONLINEAR ANALYSIS

The approach described here has been reported in detail in Reference 12, although no attention is paid there to velocity coupling. We shall not discuss the manner in which the approximations are carried out; the intent is only to note that a useful framework is available for assessing the importance of nonlinear velocity coupling.

Because the linear analysis described above has been widely useful for many years, the nonlinear analysis has been constructed to be a logical and clear generalization. The first step is to approximate the general conservation equations by treating the Mach numbers of the average and unsteady flows as small parameters. The limit process was cited earlier in equation (23). Power series expansions of the dependent variables (pressure, velocity, etc.) lead to a system of equations which can be manipulated to give a wave equation and boundary condition for the pressure fluctuation. These have the same form as equations (24) and (25), except that the functions h and f are now nonlinear in both the pressure and velocity fluctuations:

$$\nabla^2 p' - \frac{1}{\bar{a}^2} \frac{\partial^2 p'}{\partial t^2} = h \tag{83}$$

$$\hat{n} \cdot \nabla p' = f \tag{84}$$

The pressure and velocity fields are then expanded in series of the normal modes of the chamber, essentially a Fourier analysis in space with time-varying coefficients. After substitution of the expansion, equation (83) is integrated over the chamber and the boundary condition (54) is used. The result is a set of coupled oscillator equations for the amplitudes $\eta_n(t)$ of the normal modes:

$$\frac{d^2\eta_n}{dt^2} + \omega_n{}^2\eta_n = F_n \tag{85}$$

where η_n is the coefficient of the nth term in the representation

$$p' = \bar{p}\sum_{n=0}^{\infty}\eta_n(t)\hat{p}_n(\vec{r}) \tag{86}$$

The forcing function F_n is

$$F_n = \frac{\bar{a}^2}{\bar{p}E_n{}^2}\{\int\hat{h}\hat{p}_u dV + \oiint\hat{f}\hat{p}_n dS\} \tag{87}$$

and

$$E_n{}^2 = \int\hat{p}_n{}^2 dV \tag{88}$$

When h' and f' are linear, the equation (85) can be solved by assuming exponential behavior in time, and the formula (30) for the wave number follows directly.

More generally, the force F_n in the equation for the nth mode, or oscillator, depends nonlinearly on η_n itself and also the amplitudes of all the other modes. Thus the unsteady motions in the chamber are represented as a system of oscillators coupled by nonlinear interactions. The interactions cause a flow of energy between the oscillators which represents the generation of harmonics in the acoustic field. Note that the formulation is not restricted to one-dimensional problems nor to any particular geometrical configuration.

After the functions F_n are set by specifying the functions h and f, (85) s a system of coupled ordinary differential equations which can be solved numerically. It is not particularly cheap to do so because the equations are second order. Considerable simplification is achieved by taking advantage of the fact that in most practical situations the waves have amplitudes which vary quite slowly - the fractional change is small in one cycle of the oscillation. A convenient procedure to follow is based on the method of averaging which reduces the system of second order equations to a set of first order equations, two for each member of (84). Write the amplitudes

$$\eta_n(t) = A_n(t) \cos(\omega_n t + \psi_n(t)) \tag{89}$$

$$= A_n(t) \sin \omega_n t + B_n(t) \cos \omega_n t$$

where A_n, F_n, A_n, B_n are slowly varying functions of time in the sense described above.

Eventually the first order equations for the A_n and B_n can be put in the form

$$\frac{dA_n}{dt} = \alpha_n A_n + \theta_n B_n + g_n \tag{90(a)}$$

$$\frac{dB_n}{dt} = \alpha_n B_n - \theta_n A_n + h_n \tag{90(b)}$$

The linear portion of F_n produces the terms containing α_n and θ_n which are now strictly constant with no dependance on the amplitude of oscillations. All nonlinear behavior is contained in the functions g_n and h_n. There is no difficulty accommodating nonlinear velocity coupling. No calculations based on this method have been published.

REFERENCES

1. Hart, R. W., Bird, J. F., and McClure, F. T. "The Influence of Erosive Burning on Acoustic Instability in Solid Propellant Rocket Motors." Progress in Astronautics and Rocketry, V. I, Solid Propellant Rocket Research, Academic Press, New York (1960), pp 423-499.

2. McClure, F.T., Bird, J.F., and Hart, R.W. "Errosive Mechanism for Nonlinear Instability in the Axial Mode of Solid Propellant Rocket Motors." ARSJ., V. 3, No. 3 (March 1962) pp. 374 - 378.

3. Bird, J.F., Hart, R.W., and McClure, F.T, "Finite Acoustic Ocillations and Errosive Burning in Solid Fuel Rockets." AIAAJ., V. 3, No. 12 (December 1965) pp. 2248 - 2256.

4. Culick, F.E.C., "A Review of Calculations for Unsteady Burning of a Solid Propellant," AIAA J., Vol. 6, No. 12 (December 1968). pp. 2241-2255.

5. Price, E.W. and Dehority, G.L., "Velocity Coupled Axial Mode Combustion Instability in Solid Propellant Rocket Motors." 2nd ICRPG/ AIAA Solid Propulsion Meeting, Anaheim, California (June 1967).

6. Culick, F.E.C., "Stability of Three-Dimensional Motions in a Combustion Chamber." Comb. Science and Technology. V. 10 (1975), pp. 109 - 124.

7. Culick, F.E.C., "Stability of Longitudinal Oscillations with Pressure and Velocity Coupling in a Solid Propellant Rocket." Comb. Science and Technology. V. 2 (1970) pp. 179 - 201.

8. Lord Rayleigh, The Theory of Sound, V. II, Dover Publications, New York, (1945).

9. Beckstead, M.W., Horton, M.D., Krashin, M., and Butcher, A.G. "Velocity Coupling Combustion Instability." Final Technical Report AFRPL-TR-75- (July 1975).

10. Micheli, P. "Investigation of Velocity Coupled Combustion Instability." Interim Report, January 1974 - June 1975, AFRPL-TR-75-54 (October 1975).

11. Levine, J.N. and Culick, F.E.C., "Numerical Analysis of Nonlinear Longitudinal Combustion Instability in Metalized Propelland Solid Rocket Motors. V. I: Analysis and Results." Ultrasystems, Inc. (1972) Technical Report AFRPL-TR-72-88.

12. Baum, J. D., Levine, R. L., and Levine, J. N., "Pulsing of Solid Propellant Rocket Motors: A Numerical and Experimental Study." AIAA 20th Aerospace Sciences Meeting (January 1982), Paper No. AIAA-82-0359.

13. Culick, F. E. C. "Nonlinear Pressure Oscillations in Combustion Chambers." Acta. Astronautica.

NOMENCLATURE

$\bar{a}$	Speed of sound
C_m	Particle loading
C_n	Coefficient in Fourier series, equation (54)
f	Frequency (cycles per second); function defined by equation (25)
h	Defined by equation (24)
k	Wave number, $k = (\omega - i\alpha)/\bar{a}$
k_n	Wave number of the n^{th} normal mode
L	Length of a chamber
m_b	Mass flux of material leaving a burning surface
M_o	Reference Mach number
n	Exponent in the burning rate low, $r \sim p^n$
$\bar{n}$	Unit normal vector
p	Pressure
δ_p	Small change of pressure
r	Linear burning rate
δ_r	Small change of burning rate
R_p	Response function for pressure coupling
R_v	Response function for velocity coupling
dS	Element of area
S_n	Coefficient in Fourier series, equation (54)
t	Time
T	Temperature
v	Velocity

dV	Volume element
z	Coordinate along axis of a chamber
α	Imaginary part of complex wave number
β	Defined by equation (57)
γ	Ratio of specific heats
ε	Amplitude of an acoustic pressure oscillation
κ	Thermal diffusivity of solid propellant
λ	Wavelength
ρ	Material density
ω	Frequency (radians per second)
Ω	Dimensionless frequency, $\Omega = \bar{r}^2\omega/\kappa$
$\bar{(\ )}$	Average value
$(\ )'$	Fluctuation including time variation
$\hat{(\ )}$	Fluctuation without time variation
$(\ )^{(r)}$	Real part
$(\ )^{(i)}$	Imaginary part
$\lvert\ \rvert$	Absolute value

Appendix A

REDUCTION OF T-BURNER DATA TO OBTAIN THE RESPONSE FUNCTION FOR VELOCITY COUPLING

The fluctuation of burning rate due to velocity coupling is written

$$\left(\frac{r'}{\bar{r}}\right)_v = R_r\left(\frac{u'}{\bar{a}}\right)_v \tag{A-1}$$

and the formula for the growth constant, the second part of equation (42) with $c_b = 0$ and $c_v = 1$, may be written

$$\alpha_{vc} = \frac{1}{2}\frac{\bar{\rho}\bar{a}^2\bar{m}_b}{\int\hat{p}_n^2 dV}\iint\left|\widehat{R_v\left(\frac{u'}{\bar{a}}\right)_v}^{(r)}\right|\frac{\hat{p}_n}{\bar{p}}\,dS \tag{A-2}$$

The circumflex $\hat{(\ )}$ denotes the part without time dependence, and superscript r, $(\ )^{(r)}$, means real part, that part which is <u>in phase</u> with the pressure. Thus, the pressure fluctuation having amplitude ε is written, equation (51):

$$\frac{p'}{\bar{p}} = \varepsilon\cos\frac{\pi z}{L}\cos\omega_1 t \tag{A-3}$$

$$\hat{p} = \varepsilon\bar{p}\cos\frac{\pi z}{L} \tag{A-4}$$

and $\hat{p}_n$ means $\hat{p}$ at the frequency ω_n of the nth normal mode. First we examine the situation when rectification is ignored.

If u' stands only for the fluctuating velocity associated with the acoustic pressure (A-3), then it is given by equation (52),

$$u' = \varepsilon\frac{\bar{a}}{\gamma}\sin\left(\frac{\pi z}{L}\right)\sin\omega_1 t \tag{A-5}$$

which is 90 degrees out of phase with the pressure fluctuation. The response function is a complex quantity which may be written according to equation (11) as

$$R_v = R_v^{(r)} + iR_v^{(i)} = |R_v|[\cos \psi_v + i \sin \psi_v] = R_v e^{i\psi_v} \quad \text{(A-6)}$$

In complex notation, (A-3) and (A-5) are

$$p' = \varepsilon \bar{p} \cos kz e^{i\omega_1 t} = \hat{p} e^{i\omega_1 t} \quad \text{(A-7)}$$

$$u' = \varepsilon \frac{\bar{a}}{\gamma} \sin kz e^{i(\omega_1 t - \pi/2)} = \hat{u} e^{i\omega_1 t} \quad \text{(A-8)}$$

where $\hat{u}$ is pure imaginary,

$$\hat{u} = -i\varepsilon \frac{\bar{a}}{\gamma} \sin kz \quad \text{(A-9)}$$

Thus (A-3) and (A-4) are the real parts of (A-7) and (A-8). The wave number k is complex, $k = (\omega - i\alpha)/\bar{a}$ of the imaginary part, the growth constant α, is given by the formula (A-2).

For use in (A-2), with $\hat{u}/\bar{a}$ entirely out of phase with the pressure, and R_v expressed by (A-6) we have (50);

$$\left[R_v\left(\frac{\hat{u}}{\bar{a}}\right)_v\right]^{(r)} = -R_v^{(i)}\left(\frac{\hat{u}}{\bar{a}}\right)_v^{(i)} \quad \text{(A-10)}$$

Comparison of (A-7) and (A-8) gives the familiar relation between acoustic pressure and velocity,

$$\hat{u} = \frac{i}{\bar{\rho}\omega_1} \frac{d\hat{p}}{dz} \quad \text{(A-11)}$$

Substitution of (A-10) and (A-12) into (A-2) leads to

$$\alpha_{vc} = -\frac{1}{2}\frac{\bar{a}^2\bar{m}_b}{\bar{\rho}\omega_1}\frac{1}{\int\hat{p}_n^2\,dV}\int\hat{p}_n\frac{d\hat{p}}{dz}\,dV \qquad \text{(A-12)}$$

For a uniform cylinder, $dV = S_c dz$ and with $\hat{p} \quad p_n$, this becomes

$$\alpha_{vc} = -\frac{1}{4}\left(\frac{\bar{a}^2\bar{m}_b}{\bar{\rho}\omega_1}\right)\frac{1}{\int_o^L \hat{p}n^2 dz}\int_o^L \frac{d\hat{p}_n^2}{dz}\,dz \qquad \text{(A-13)}$$

But because $\hat{p}_n^2$ has the same value at both ends of the chamber, the integral vanishes:

$$\int_o^L \frac{d\hat{p}_n^2}{dz}\,dz = \hat{p}_n^2(L) - \hat{p}_n^2(o) = 0$$

It is because of the different phases between the velocity and pressure fluctuations that there is no influence of velocity coupling in this case; see Figures 5 and 7 for examples.

The main point is that <u>if</u> rectification is ignored <u>and</u> the configuration is symmetric (this was implied in carrying out the integral above) <u>then</u> there is no influence of velocity coupling. So now we must account for rectification.

We assume that the threshold velocity is zero and write the velocity effective in velocity coupling as equation (53):

$$\left(\frac{u'}{\bar{a}}\right)_v = \frac{1}{\bar{a}}\left|\bar{u} + u'\right| - \frac{1}{\bar{a}}\left|u\right| \qquad \text{(A-14)}$$

The first term $|\bar{u} + u'|$, accounts for the rectification with unsteady flow, and the second term ensures that the effect vanishes when there is no fluctuation ($u' = o$). We must now determine that part of (A-14)

which is out of phase with the pressure fluctuation, that is, oscillates with the time dependence sin ωt, and has the same frequency as the pressure fluctuation.

To accomplish this most easily, expand (A-14) in Fourier series, formally written as equation (54),

$$\left(\frac{u'}{\bar{a}}\right)_v = C_o + \sum_{n=1}^{\infty} C_n \cos(n\omega_1 t) + \sum_{n=1}^{\infty} S_n \sin n\omega_1 t \qquad \text{(A-15)}$$

where the coefficients are given by the formulas

$$C_o = \frac{1}{2\pi} \int_o^{2\pi} \left(\frac{u'}{\bar{a}}\right)_v d(\omega_1 t) \qquad \text{(A-16)}$$

$$C_n = \frac{1}{\pi} \int_o^{2\pi} \left(\frac{u'}{\bar{a}}\right)_v \cos(n\omega_1 t)\, d(\omega_1 t) \qquad \text{(A-17)}$$

$$\frac{1}{\pi} \int_o^{2\pi} \left(\frac{u'}{\bar{a}}\right)_v \sin(n\omega_1 t)\, d(\omega_1 t) \qquad \text{(A-18)}$$

As remarked after equation (54), only the coefficients C_1 and S_1 are required.

The coefficients C_n and S_n are given in the main text, equations (63) through (67) for the case when the threshold velocity is assumed to vanish and the mean-flow speed $\bar{u}$ is positive, implying flow to the right. Equation (66) for B_1 is

$$S_1 = \frac{\bar{u}}{\bar{a}} \frac{4}{\pi} \left\{ \sin\sigma + \beta \left| 1 - \frac{2}{\pi}\sigma - \frac{1}{\pi}\sin 2\sigma \right| \right\} \qquad \text{(A-19)}$$

where $\cos \sigma = 1/\beta$ when $\beta > 1$ and $\sigma = 0$ if $\beta \leq 1$. The case $\sigma \neq 0$ arises when rectification occurs, otherwise, $\beta \leq 1$ according to the definition (58),

$$\beta = \frac{\varepsilon \bar{a}}{\gamma u} \sin\left(\frac{\pi z}{L}\right) \tag{A-20}$$

That is, β, is the ratio of the local amplitude of the acoustic velocity for the local mean-flow speed. In $\sigma = 0$, $S_1 = \bar{u}\beta$ and (A-10) becomes

$$\left[R_v \frac{\hat{u}}{\bar{a}}\right]^{(r)} = -\frac{R_v^{(i)}}{\bar{p}\omega_1} \frac{d\hat{p}}{dz} = R_v^{(i)} \frac{\varepsilon}{\gamma} \sin\left(\pi \frac{z}{L}\right) \tag{A-21}$$

Substitution into (A-2) correctly produces (A-13) again.

We now consider the procedure for calculating α_{vc} associated with oscillations in a T-burner. For simplicity we treat only the case of a burner having a center vent and symmetrical configurations of grains. End grains may be installed to provide average flow part test grains, and additional pressure-coupled driving of instabilities. The following analysis is intended only to give results for the contributions due to velocity coupling with symmetrically placed cylindrical test grains. It is not a comprehensive analysis of the T-burner.

For each test sample, the distribution of mean-flow speed and the acoustic velocity must be known. The latter may be calculated from the formula (A-4) for the acoustic pressure. The sketches in Figure A-1 show typical distributions of the acoustic and mean-flow velocities for samples on two sides of a T-burner. The acoustic velocity is drawn for the portion of a cycle when the oscillatory motion is everywhere to the right.

Note that the signs must be correctly accounted for so we must consider the case when $\bar{u}$ and u' have opposite signs. For $\bar{u}$ negative, replace $\bar{u}$ by $-\bar{u}$ in the formula (A-14) to find

$$\frac{1}{\bar{u}} \left| |u'| - |\bar{u}| \right| = |\beta \sin \omega t - 1| \tag{A-22}$$

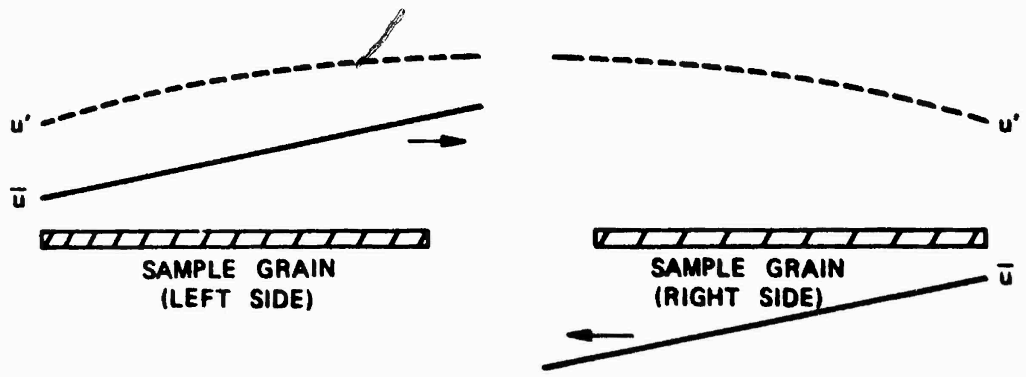

FIGURE A-1. Mean and Fluctuating Velocities for Two Sample Grains in a T-Burner.

where β is defined by (60) with $|\bar{u}|$ replacing $\bar{u}$. A sketch of (A-22) for $\bar{u} < 0$ is given in Figure A-2. This corresponds to the sketch in Figure 13 for $\bar{u}$ positive, and is obtained by reflecting $|\beta \sin \omega_1 t + 1|$ about the origin, and then shifting by $+2\pi$. The piecewise representation is

$$|\beta \sin \omega t - 1| = 1 - \beta \sin \omega_1 t \qquad 0 \leq \omega_1 t \leq \sigma$$

$$= \beta \sin \omega_1 t - 1 \qquad \sigma \leq \omega_1 t \leq \frac{\pi}{2} + \sigma$$

$$= 1 - \beta \sin \omega_1 t \qquad \frac{\pi}{2} + \sigma < \omega_1 t \leq 2\pi$$

The value of σ is the same as for the case $\bar{u} > 0$ because here the condition is $\beta \sin (\frac{\pi}{2} - \sigma) = 1$ which gives $\cos \sigma = 1/\beta$ as in equation (58). Again the interesting cases arise for $\beta > 1$; the first three coefficients in the Fourier expansion are:

$$\bar{u} < 0 \; ; \; \beta > 1$$

$$C_1 = \frac{\bar{u}}{\bar{a}} \frac{2}{\pi} |\beta \sin \sigma - \sigma| \qquad \text{(A-23)}$$

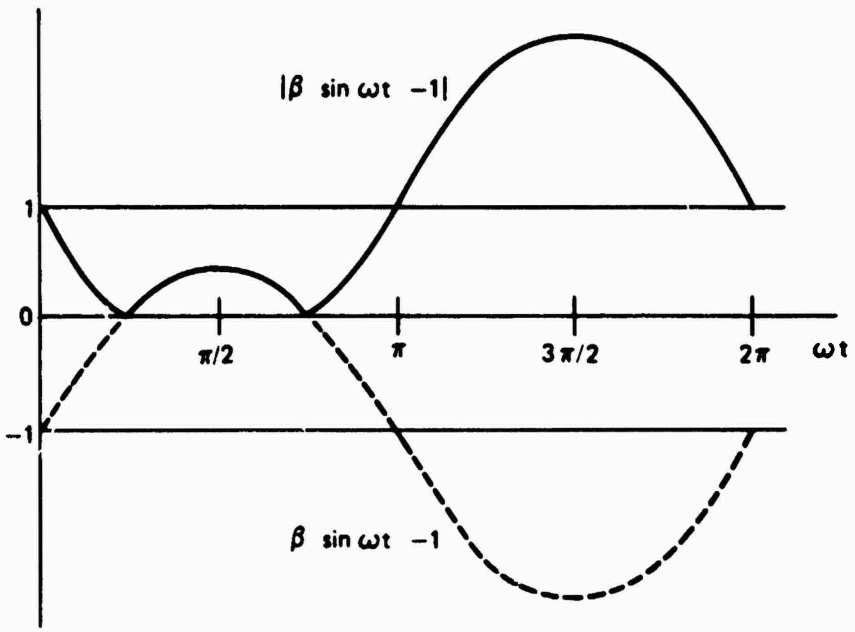

FIGURE A-2. One Cycle of a Rectified Waveform for Mean Flow in the Negative Direction.

$$C_2 = 0 \tag{A-24}$$

$$S_1 = -\frac{|\bar{u}|}{\bar{a}} \left\{ \frac{4}{\pi} \sin\sigma + \beta \left| 1 - \frac{2}{\pi}\sigma - \frac{1}{\pi}\sin 2\sigma \right| \right\} \tag{A-26}$$

The average value, C_o, is the same as for the case $\bar{u}$ positive, as a comparison of Figures 13 and A-2 shows immediately. However, the value of S_1 for $\bar{u} < 0$, which is the case in the right half of a T-burner, is exactly the negative of that given by equation (A-19) for $\bar{u} > 0$. Hence, for use in (A-2), the formula (55) is

$$\left[R_v \frac{u}{a} \right]^{(r)}_{v} = \frac{\bar{u}}{\bar{a}} R_v^{(i)} \begin{cases} S \text{ (left half)} \\ -S \text{ (right half)} \end{cases} \tag{A-27}$$

where

$$S = \frac{4}{\pi} \sin \sigma + \beta\left\{1 - \frac{2}{\pi}\sigma - \frac{1}{\pi} \sin 2\sigma\right\} \qquad \text{(A-28)}$$

Strictly, the integral in (A-2) must be carried out over the sample grains, but as a first approximation for quick reduction of data, it is adequate to use average values. We assume that the samples are at $z = L/4$ and $z = 3L/4$. By symmetry, $\bar{u}$ has the same values at the two locations. If the areas of the samples are each S_{ev}, then the surface integral in (A-2) is approximately

$$\oint\!\!\oint \overbrace{\left[R_v\left(\frac{u'}{\bar{a}}\right)_v\right]}^{(r)} p_n dS \cong S_{lv} R_v^{(i)} \left| (S_l \hat{p}_n)_{L/4} + (S_l \hat{p}_n)_{3L/4} \right|$$

$$= \varepsilon \bar{p} S_{lv} R_v^{(i)} \left| \bar{u}\, S \cos\frac{\pi}{4} - |\bar{u}| S \cos\frac{3\pi}{4} \right|$$

$$= \varepsilon \bar{p} \sqrt{2}\, S_{lv} R_v^{(i)} S$$

With S given by (A-28)

$$\oint\!\!\oint \overbrace{\left[R_v\left(\frac{u'}{\bar{a}}\right)_v\right]}^{(r)} \frac{\hat{p}_n}{\bar{p}}\, dS = \varepsilon \frac{|\bar{u}|}{\bar{a}} S_{ev} R_v^{(i)} \sqrt{2}\left[\frac{4}{\pi} \sin\sigma + \beta\left\{1 - \frac{2\sigma}{\pi} - \frac{\sin 2\sigma}{\pi}\right\}\right] \qquad \text{(A-29)}$$

Because $\int p_n^2 dV = \varepsilon^2 \bar{p}^2 \frac{S_c L}{2}$, the formula (A-2) is finally

$$\sigma_{vc} = \sqrt{2}\left(\frac{S_{ev}}{S_c}\right)\left(\frac{\bar{u}}{L}_{ave}\right)\left(\frac{\bar{a}\bar{m}_b}{\varepsilon \bar{p}}\right) R_v^{(i)}\left[\frac{4}{\pi} \sin\sigma + \beta\left\{1 - \frac{2\sigma}{\pi} - \frac{\sin 2\sigma}{\pi}\right\}\right] \qquad \text{(A-30)}$$

Both β, equation (A-20), and therefore $\sigma = \cos^{-1} 1/\beta$ are based on the value of $\bar{u}$ averaged over the propellant sample.

INITIAL DISTRIBUTION

10 Naval Air Systems Command
- AIR-00D4 (2)
- AIR-03A (1)
- AIR-32 (1)
- AIR-320 (1)
- AIR-330 (1)
- AIR-522 (1)
- AIR-5312 (1)
- AIR-536 (1)
- AIR-6301 (1)

2 Chief of Naval Material
- NSP-27 (1)
- NSP-2731 (1)

5 Naval Sea Systems Command
- SEA-62 (1)
- SEA-62B (1)
- SEA-62R (1)
- SEA-99612 (2)

1 Commander in Chief, U.S. Pacific Fleet (Code 325)
1 Marine Corps Development and Education Command, Quantico (Marine Corps Landing Force Development Center)
1 Air Test and Evaluation Squadron 5
1 Commander, Third Fleet, Pearl Harbor
1 Commander, Seventh Fleet, San Francisco
1 Fleet Analysis Center, Naval Weapons Station, Seal Beach, Corona (Library)
1 Naval Air Development Center, Warminster (Code 606)
1 Naval Explosive Ordnance Disposal Technology Center, Indian Head
1 Naval Intelligence Support Center (NISC-60, Library)
1 Naval Ocean Systems Center, San Diego (Code 133)
3 Naval Ordnance Station, Indian Head
- Code 515, P. L. Stang (1)
- Code 52 (1)
- Technical Library (1)

1 Naval Postgraduate School, Monterey (Department of Aeronautics, D. W. Netzer)
1 Naval Research Laboratory (Code 432, R. S. Miller)
3 Naval Ship Weapon Systems Engineering Station, Port Hueneme
- Code 5711, Repository (2)
- Code 5712 (1)

4 Naval Surface Weapons Center, Dahlgren
- G20 (1)
- G20, J. L. East, Jr. (1)
- DG (1)
- DG50 (1)

5 Naval Surface Weapons Center, White Oak Laboratory Silver Spring
- R11 (1)
- R16 (1)
- R16, C. B. Wilmot (1)
- R17 (1)
- Technical Library (1)

1 Naval Intelligence Support Center Liaison Officer (LNN)

1 Naval War College, Newport
1 Naval Weapons Support Center, Crane (Code 5042)
1 Navy Strategic Systems Projects Office (SP 2731, E. L. Throckmorton, Jr.)
1 Army Armament Materiel Readiness Command, Rock Island (DRSAR-LEM)
7 Army Armament Research and Development Command, Dover
  DRDAR-LCA-G
    D. S. Downs (1)
    J. A. Lannon (1)
  DRDAR-LCN-C, Concepts & Analysis Branch (4)
  DRDAR-SCA-T, L. Stiefel (1)
2 Army Missile Command, Redstone Arsenal (DRSMI-RK, D. J. Ifshin)
4 Army Ballistic Research Laboratory, Aberdeen Proving Ground
  DRDAR-BLI, I. W. May (3)
  DRDAR-TSB-S (STINFO) (1)
2 Air Force Systems Command, Andrews Air Force Base
  DLFP (1)
  SDZ (1)
1 Air Force Wright Aeronautical Laboratories, Wright- Patterson Air Force Base (AFWAL/PORA)
4 Air Force Armament Laboratory, Eglin Air Force Base
  AFATL/DLDE (1)
  AFATL/DLDL, O. K. Heiney (1)
  AFATL/DLMI, Mr. Aden (1)
  AFATL/DLODL (1)
1 Air Force Rocket Propulsion Laboratory, Edwards Air Force Base (Code MKCC)
1 Air Force Rocket Propulsion Laboratory, Edwards Air Force Base (Code MKP)
5 Air Force Rocket Propulsion Laboratory, Edwards Air Force Base (PACC, W. E. Roe)
1 Air Force Rocket Propulsion Laboratory, Edwards Air Force Base (Technical Library)
1 Bolling Air Force Base (L. H. Caveny)
2 Foreign Technology Division, Wright-Patterson Air Force Base
  FTD/SDNW, J. Woodard (1)
  FTD/TQFA, Kern (1)
1 Defense Advanced Research Projects Agency, Arlington
12 Defense Technical Information Center
1 Lewis Research Center, (NASA), Cleveland, OH
1 George C. Marshall Space Flight Center (EP 25, J. Q. Miller)
1 Lyndon B. Johnson Space Center (EP, H. O. Pohl)
1 AVCO Research Laboratory, Everett, MA (D. B. Stickler)
2 Aerojet Tactical Systems, Sacramento, CA, Via AFPRO (M. J. Ditore, Bldg. 2019, Dept. 3010)
2 Aerospace Corporation, Los Angeles, CA
  E. M. Landsbaum, M4-968 (1)
  Library (1)
1 Arvin Calspan, Advanced Technology Center, Buffalo, NY (E. B. Fisher)
1 Atlantic Research Corporation, Alexandria, VA (M. K. King)
1 Atlantic Research Corporation, Gainesville, VA (R. H. W. Waesche)
1 Battelle Memorial Laboratory, Tactical Technology Information Center, Columbus, OH (J. Huggins)
1 California Institute of Technology, Pasadena, CA (MC 301-46, F. E. C. Culick)
1 California Institute of Technology, Jet Propulsion Laboratory, Pasadena, CA (MS 125 159, L. D. Strand)
3 Georgia Institute of Technology, Atlanta, GA (School of Aerospace Engineering, E. W. Price)
3 Hercules Incorporated, Allegany Ballistics Laboratory, Cumberland, MD (R. R. Miller)
1 Hercules Incorporated, Eglin Air Force Base, Via AFPRO (AFATL/DLDL R. L. Simmons)
3 Hercules Incorporated, Magna, UT, (K. P. McCarty)
1 Hercules Incorporated, McGregor, TX (W. F. Brooks)
1 Johns Hopkins University, Applied Physics Laboratory, Chemical Propulsion Information Agency, Laurel, MD (T. W. Christian)

2 Lockheed Palo Alto Research Laboratory, Palo Alto, CA
Department 52-35/B204/2
G. Lo (1)
H. Marshall (1)
1 Princeton Combustion Research Laboratories, Princeton, NJ (N. A. Messina)
1 Princeton University, Forrestal Campus Library, Princeton, NJ
(MAE Department, Eng. Quad, F. A. Williams, D325)
1 Purdue University, West Lafayette, IN (School of Aeronautics and
Astronautics, J. R. Osborn, Grissom Hall)
1 Rockwell International Corporation, Canoga Park, CA (J. E. Flanagan/HB02)
1 Science Applications, Inc., Chatsworth, CA (R. B. Edelman)
1 Science Applications, Inc., Princeton, NJ (H. S. Pergament)
2 Software & Engineering Associates, Inc., Santa Ana, CA (D. E. Coats)
1 TRW Inc., Redondo Beach, CA (Space and Technology Group, A. C. Ellings)
1 The Boeing Aerospace Co., Research & Engineering Division, Seattle, WA
(D. Brunner, MS 85-13)
1 Thiokol Corporation, Elkton Division, Elkton, MD (W. N. Brundige)
3 Thiokol Corporation, Huntsville Division, Huntsville, AL (R. O. Hessler)
3 Thiokol Corporation, Wasatch Division, Brigham City, UT (J. A. Peterson)
1 United Technologies Corporation, Chemical Systems Division, Sunnyvale, CA
(R. S. Brown)
2 United Technologies Research Center, East Hartford, CT (Document Control Station, J. B. McVey)
1 Universal Propulsion Company, Inc., Phoenix, AZ (H. J. McSpadden)
1 University of Illinois, Urbana, IL (ME/IE Department, H. Krier,
144 ME Bldg.)
110 Chemical Propulsion Mailing List dated December 1981 including categories 1, 2, 3, 4, 5